4-1-1997

Chemistry of the Jovian Auroral Ionosphere

J. J. Perry

Y. H. Kim

Jane L. Fox
Wright State University - Main Campus, jane.fox@wright.edu

H. S. Porter

JOURNAL OF GEOPHYSICAL RESEARCH, VOL. 104, NO. E7, PAGES 16,541–16,565, JULY 25, 1999

Chemistry of the Jovian Auroral Ionosphere

J. J. Perry[1]
Department of Physics, Wright State University, Dayton, Ohio

Y. H. Kim[2] and J. L. Fox[3]
Marine Sciences Research Center, State University of New York at Stony Brook

H. S. Porter
Department of Computer Science, Furman University, Greenville, South Carolina

Abstract. We have investigated the chemistry of the Jovian auroral thermosphere-/ionosphere by modeling the precipitation of high-energy electrons into the auroral zones using a multistream electron-transport code and three model thermospheres: a standard model based on pressure and temperature data from Galileo, and two additional models that are characterized by enhanced eddy diffusion coefficients. We have predicted the effects of precipitation of monoenergetic electrons with energies between 20 and 100 keV with energy fluxes of about 11 ergs $cm^{-2}s^{-1}$. We have derived the column densities of H_2, H, CH_4, and C_2H_2 above the altitudes of peak energy deposition. For methane column densities similar to those determined from IUE and Hubble Space Telescope H_2 spectral data, we find that for our standard model, the most likely electron energies are in the 45–55 keV range. For the enhanced eddy diffusion models the energies are lower. We present ion density profiles, H density profiles, and production profiles for the most important H_2 and H emissions. The predicted H column densities are in the range $(1-6)\times10^{18}$ cm^{-2} for the standard model and are smaller for the enhanced eddy diffusion models. We find that the temperatures near the altitude of peak energy deposition vary from 160 to 200 K and are significantly lower than those derived from rotational analyses of auroral H_2 emissions, which average 400–500 K. This indicates that the auroral thermosphere is considerably warmer than those at lower latitudes that were measured by the Voyager spacecraft or the Galileo probe.

1. Introduction

Precipitation of high-energy particles into the auroral regions of a planet may have significant effects on the chemical and thermal structure of that region. On Jupiter, the power of the aurora inferred from the ultraviolet emission rates is in the range $10^{13}-10^{14}$ W [e.g., *Sandel et al.*, 1979; *Broadfoot et al.*, 1981; *Yung et al.*, 1982; *Gérard and Singh*, 1982; *Waite et al.*, 1983; *Skinner et al.*, 1984; *Morrissey et al.*, 1997] and is larger than that of the total extreme ultraviolet solar input over the entire sunlit hemisphere. It has been proposed that this auroral energy input, which manifests itself as chemical energy, luminosity, and heating, affects the entire Jovian thermosphere, perhaps in profound ways [e.g., *Gérard and Singh*, 1982; *Waite et al.*, 1983; *Clarke et al.*, 1994]. The major forms of auroral luminosity are the H_2 Lyman ($B^1\Sigma_u^+ \rightarrow X^1\Sigma_g^+$) and Werner ($C^1\Pi_u \rightarrow X^1\Sigma_g^+$) bands, which appear in the far ultraviolet (FUV), H Lyman alpha at 1216 Å, emission from H_3^+ ν_2 fundamental and overtone bands near 4 and 2 μm, respectively [e.g., *Drossart et al.*, 1989, 1993a; *Oka and Geballe*, 1990; *Miller et al.*, 1990], and infrared emissions from hydrocarbon molecules [*Caldwell et al.*, 1980, 1983; *Kim*, 1988], some of which have been observed to be enhanced relative to their midlatitude values. In addition, quadrupole emission from $H_2(v=1\rightarrow0)$ near 2 μm has been measured from the auroral regions [*Kim et al.*, 1990]. X-ray emissions from the polar regions of Jupiter have been detected with the Einstein Observatory [*Metzger et al.*, 1983] and with the Röntgen Satellite [*Waite et al.*, 1994]. A possible visible aurora was observed by the imaging experiment on board Voyager 1 [*Cook et al.*, 1981], and recently the

[1]Now at AODTRA/CPTIP, Kirtland AFB, New Mexico.
[2]Also at Chungnam National University, Daejon, Korea.
[3]Also at Wright State University, Dayton, Ohio.

Paper number 1999JE900022.
0148-0227/99/1999JE900022$09.00

first spatially resolved images of the visible aurora were made by the Galileo Solid-State Imaging Camera [*Ingersoll et al.*, 1998].

The particles that produce the Jovian auroral emissions have not been definitively identified, but it appears that electrons with energies of 10 to 100 keV are the most likely source of the majority of the observable emissions, although heavy ions and protons may also make some contributions. Images of the FUV auroral emissions taken with the Hubble Space Telescope (HST) Wide Field Planetary Camera 2 show that the oval is magnetically connected to middle magnetosphere and is distinct from the Io footprint, which may be produced by precipitation of electrons or of the Iogenic heavy ions O^+ and S^+ [*Clarke et al.*, 1996]. In addition, the absence of the $O(^3S^o \rightarrow ^3P)$ triplet at 1304 Å in auroral spectra limits the role of O^+ in producing the observed emissions [*Waite et al.*, 1988]. Upper limits were placed on the contribution of S^+ from the intensities of possible weak sulfur emissions in IUE spectra [*Waite et al.*, 1988] and in spectra obtained with the Hopkins Ultraviolet Telescope (HUT) [*Morrissey et al.*, 1997]. *Clarke et al.* [1989] found no evidence for strongly Doppler-shifted Lyman alpha emission in a series of high-dispersion IUE spectra. Such emission would be present if high-energy proton precipitation played a significant role in the auroral excitation. Recently, more stringent upper limits were placed on the role of precipitation of heavy ions by *Trafton et al.* [1998], who searched for evidence of precipitating O^+ and S^+ and ambient thermal ions in HST spectra from 1250 to 1680 Å but found none.

There have been only a few discussions of the chemical effects of precipitating electrons in the Jovian auroral regions. *Gérard and Singh* [1982] used the continuous slowing down approximation to model the ion production, excitation rates, and heating in the auroral regions due to precipitating electrons. The initial energy distributions of the electrons were assumed to be Maxwellian with characteristic energies of 0.1, 0.4, 2, and 10 keV. H^+, H_2^+, and H_3^+ density profiles were presented for 2 keV electrons incident with an energy flux of 1 erg $cm^{-2}s^{-1}$. *Waite et al.* [1983] carried out a comprehensive study of the effects of solar EUV and precipitation of energetic electrons on the ion and neutral densities, the auroral emission rates, and plasma and neutral temperatures of the Jovian thermosphere and ionosphere. They modeled precipitation of monoenergetic 1 keV and 10 keV electrons using a two-stream electron-transport code and a background model atmosphere based on Voyager measurements. The assumed energy flux, 10 ergs $cm^{-2}s^{-1}$, was chosen to produce about 80 kR of emission in the H_2 Lyman and Werner bands [*Sandel et al.*, 1979]. Waite et al. computed the densities of H and H^+ including both chemistry and transport, and carried out photochemical equilibrium calculations for 10 other ions. Density profiles were presented, however, only for the neutral species and for electrons.

At the time of the *Waite et al.* [1983] study, absorption of the H_2 emissions by methane and other hydrocarbons was thought to be minimal. *Durrance et al.* [1982] compared the spectra of the Jovian auroral regions taken with the International Ultraviolet Explorer (IUE) to that of an H_2 discharge lamp and found no evidence for absorption of the H_2 emissions by methane. *Yung et al.* [1982] compared IUE spectra to a model spectrum and defined two "color ratios," one of which indicated that the precipitating particles penetrated the methane homopause slightly. They suggested that electrons with energies of about 10 keV deposit their energy in the region of the homopause and that the precipitating electrons therefore were most likely characterized by energies in the 1–30 keV range. *Herbert et al.* [1987] used Voyager auroral spectra to estimate a modest column abundance of hydrocarbons at the peak of the emission region of $(1-5) \times 10^{15}$ cm^{-2} and inferred precipitating electron energies also of $1-30$ keV, with lower values preferred. By fitting laboratory spectra of H_2 emissions modified by transmission functions of CH_4 and C_2H_2 to two IUE spectra, *Waite et al.* [1988] concluded that the precipitating particles deposit their energy just above the methane homopause. For electrons as the primary particles, they estimated energies in the 10–30 keV range.

Gladstone and Skinner [1989], however, compared two IUE spectra in the 1200–1700 Å wavelength region to detailed synthetic spectra and suggested that the precipitating particles penetrated the homopause to a significantly larger methane column density of about 5×10^{16} cm^{-2}. For a model of the north equatorial belt based on Voyager data, the depth of penetration of the particles was determined to be about 1.8×10^{21} H_2 cm^{-2}, and an electron energy of about 95 keV was derived. Although their synthetic spectra were sophisticated, Gladstone and Skinner assumed that the precipitating electron energy deposition followed a simple Chapman profile.

Livengood et al. [1990] used 229 FUV spectra of the Jovian auroral regions obtained with IUE from 1978 to 1989 to study the temporal and spatial variations of methane optical depth and intensity. In addition to their "equatorial model," which was based on Voyager data, they constructed a simple isothermal "polar model," which was characterized by a higher methane homopause. They did not carry out an electron transport calculation but made the approximation that the electrons deposit their energy in a narrow altitude region. The derived range for the precipitating electron energies was 9–17 keV for the polar model and 24–49 keV for the equatorial model, and they found a correlation between greater extinction and greater intensities.

Singhal et al. [1992] computed UV intensities in the Lyman and Werner bands, and density profiles for 24 ions due to precipitation of energetic electrons in Maxwellian energy distributions with characteristic energies of 10, 30, and 100 keV, and energy fluxes of 10

ergs $cm^{-2}s^{-1}$ into the Jovian auroral region. The background model atmosphere for the electron energy deposition calculation contained H_2, He, and H, and the electron energy loss was modeled using the continuous slowing down approximation. For the excitation and ionization rate calculation, methane was added to the atmosphere, with the density profile taken from the polar model of *Livengood et al.* [1990]. The chemistry calculations included, in addition, CH_3, C_2H_2, C_2H_4, and C_2H_6, with fixed density profiles taken from Voyager data [*Atreya*, 1986] and the calculations of *Gladstone* [1982a]. Singhal et al. assumed that ions other than H^+ were in photochemical equilibrium, and they presented the first detailed density profiles of hydrocarbon ions with up to two carbon atoms, with the C_3 and C_4 ions treated as a class.

Recently, *Rego et al.* [1994] computed excitation rates for H Lyman alpha and the Lyman and Werner band systems of H_2 due to precipitating protons and electrons of energies 10–50 keV using the continuous slowing down approximation. Ion densities were not reported, and the other effects of the precipitating particles were not assessed.

We investigate here the effects of electron precipitation into the Jovian auroral regions for a model based on Galileo and Voyager data. We have carried out complete electron transport calculations of the effects of precipitating electrons with a range of energies from 20 to 100 keV. We present excitation, dissociation, and ionization rates and compute the density profiles of 21 ions (H^+, H_2^+, H_3^+, He^+, HeH^+, C^+, CH^+, CH_2^+, CH_3^+, CH_4^+, CH_5^+, C_2^+, C_2H^+, $C_2H_2^+$, $C_2H_3^+$, $C_2H_4^+$, $C_2H_5^+$, $C_2H_6^+$, $C_2H_7^+$, $C_3H_n^+$, and $C_4H_n^+$, where the latter two ions represent classes of ions with three or more and four or more carbon atoms, respectively) and eight minor neutral species (CH, $^1CH_2$, $^3CH_2$, CH_3, C_2H, C_2H_3, C_2H_5, and H) simultaneously. In addition to chemistry, transport by molecular and eddy diffusion is included for neutrals, and ambipolar diffusion is included for ions. We discuss the auroral production and loss of H, and the resulting H density profiles, and compare them to those inferred from recent observations of the Jovian auroral Lyman alpha line profile [*Prangé et al.*, 1997]. We also model the rates of production of the excited states of H_2 and H that are responsible for the observed auroral UV and visible emissions. Finally, we compare the temperatures at the altitudes of maximum energy deposition to those inferred from HST spectra.

2. Calculations

We have carried out electron transport calculations using a multistream electron-transport code written by H. S. Porter [e.g., *Porter et al.*, 1987]. The electrons were assumed to be monoenergetic with energies of 20, 30, 40, 50, 65, 75, 85, 92 and 100 keV and energy fluxes of about 11 ergs $cm^{-2}s^{-1}$. The energy fluxes were normalized to that required to produce 60 kR of Lyman band emission before absorption by methane, a typical value obtained in the HST Goddard High Resolution Spectrograph (GHRS) observations of *Kim et al.* [1997] (80 kR) after correction by the factor of 0.725 for a diffuse source [*Space Telescope Science Institute*, 1994]. The precipitating electron flux was assumed to be isotropic over the downward hemisphere, and the steady state fluxes were computed for 20 streams of electrons. In the electron energy loss calculations, we have included electron impact on H_2, He, H, CH_4, C_2H_2, C_2H_4, and C_2H_6. The inelastic cross sections have been updated, and their sources are presented in Table 1. Elastic scattering of electrons from H_2, He, and H was included, with the same cross sections as those employed by *Kim et al.* [1992]. The auroral region was assumed also to be sunlit, with a solar zenith angle of 60°. Photoabsorption by H_2, H, He, CH_4, C_2H_2, C_2H_4, and C_2H_6 was included, and the cross sections adopted were the same as those compiled by *Kim and Fox* [1994]. The photoelectron energy deposition was carried out with the approximation that these low-energy electrons lose their energy locally.

To compute the steady state ion density profiles, 161 ion-molecule reactions were included, with rate coefficients taken mainly from the evaluation by *Anicich* [1994]. Many of the rate coefficients that have been used are the same as those listed by *Kim and Fox* [1994]; the rate coefficients that have been changed, along with other reactions that we refer to in the discussion, are shown in Table 2. A few of these deserve comment. The rate coefficient for reaction (R1)

$$H_2^+ + He \rightarrow HeH^+ + H \quad (1)$$

was previously assumed to be $1.4 \times 10^{-10}\,cm^3\,s^{-1}$. The reaction is endothermic by about 19 kcal/mol, however, and the rate coefficient recommended by *Anicich* [1994] applies only to suprathermal collision energies. We have therefore set the rate coefficient for the above reaction to zero in this study. Reaction (R15)

$$C_2H_2^+ + H_2 \rightarrow C_2H_3^+ + H \quad (2)$$

also appears to be slightly endothermic by about 2 kcal/mol, and the rate coefficient for the reverse (exothermic) reaction is $1 \times 10^{-10}\,cm^3\,s^{-1}$ [*Hansel et al.*, 1989]. We have adopted a rate coefficient of $1 \times 10^{-10} \exp(-800/T)\ cm^3\,s^{-1}$, rather than the temperature independent value $1 \times 10^{-12}\,cm^3\,s^{-1}$ assumed previously. Similarly, reaction (R11)

$$CH_5^+ + H \rightarrow CH_4^+ + H_2 \quad (3)$$

is endothermic by 2.9 kcal/mol and the rate coefficient for the reverse (exothermic) reaction is $3 \times 10^{-11}\,cm^3\,s^{-1}$ [*Federer et al.*, 1985]. We have here adopted a rate coefficient of $3 \times 10^{-11} \exp(-1460/T)\ cm^3\,s^{-1}$.

Forty ion recombination reactions have been included. Those whose rate coefficients have been modified since

Table 1. Electron Impact Cross Sections

Species	Processes	References
H_2	ionization	*Rapp and Englander-Golden* [1965]
	$B\ ^1\Sigma_u^+$, $B'\ ^1\Sigma_u^+$, $B''\ ^1\Sigma_u^+$	A. Dalgarno (private communication, 1996)
	$C\ ^1\Pi_u$, $D\ ^1\Pi_u$, $D'\ ^1\Pi_u$	based on *Liu et al.* [1998] and *Abgrall et al.* [1993a, b]
	$E,F\ ^1\Sigma_g^+$	*Shemansky et al.* [1985], *Ajello et al.* [1988]
	$c\ ^3\Pi_u$, $a\ ^3\Sigma_g^+$	*Mason and Newell* [1986]
	$b\ ^3\Sigma_u^+$	*Lima et al.* [1985]
	$3p\ ^3\Pi_u$	*Möhlmann and De Heer* [1976]
	H Lyman α	*Ajello et al.* [1991]
	H($2s$)	*Ajello et al.* [1988], *Mumma and Zipf* [1971]
	Balmer-α, β, γ	*Möhlman et al.* [1978], *Freund et al.* [1976]
	v= 0 → 1, 2, 3, 4, 5, 6	*Allan* [1985], *Ehrhardt et al.* [1968]
	rotational excitation	
	J=0 → 2	*Gibson* [1970]
	J=1 → 3	*Linder and Schmidt* [1971]
H	ionization	*De Heer et al.* [1977, and references therein]
	$2s$, $2p$	*Scott et al.* [1989]
	$3s$, $3p$, $3d$	*Callaway and Unnikrishnan* [1993]
He	ionization	*Jackman et al.* [1977]
	excitation	*Jackman et al.* [1977]
CH_4	ionization	*Rapp and Englander-Golden* [1965]
	El. Exc1, El. Exc2	*Vuskovic and Trajmar* [1983]
	CH,H_2,H	*Winters* [1975], *Adamczyk et al.* [1966]
	CH(A→X), Balmer-α	*Möhlmann and De Heer* [1977]
	CI(1657), CI(1931)	*Pang et al.* [1987]
	vibrational excitation	
	ν_1 and ν_3, ν_2 and ν_4	*Tanaka* [1984], *Duncan and Walker* [1972]
C_2H_2	ionization	*De Heer* [1981], *Zeng and Srivastava* [1996]
	CH(A→X), Balmer-α	*Möhlmann and De Heer* [1977]
C_2H_4	ionization	*Rapp and Englander-Golden* [1965] *Phillips Petroleum Co.* [1983]
	CH(A→X), Balmer-α	*Möhlmann and De Heer* [1977]
C_2H_6	ionization	*De Heer* [1981], *Chatham et al.* [1984]
	CH(A→X), Balmer-α	*Möhlmann and De Heer* [1977]

the study of *Kim and Fox* [1994] and their sources are given in Table 3. One of the most important dissociative recombination reactions is that of H_3^+, which may proceed via two possible channels (reactions (RC1) and (RC2)):

$$H_3^+ + e \rightarrow H_2 + H \quad (4)$$

$$\rightarrow H + H + H \quad (5)$$

The rate coefficient, which was believed for a time to be quite small, 10^{-8} $cm^3\,s^{-1}$ or less, for H_3^+ in the ground vibrational state (see the review by *Mitchell* [1990]), has been measured by several groups and more recently found to be of the order of $10^{-7}\,cm^3\,s^{-1}$. We adopt here the value $1.15 \times 10^{-7}(300/T)^{0.65}\,cm^3\,s^{-1}$ reported by *Sundström et al.* [1994]. The yield of the two channels in dissociative recombination of H_3^+ has also been measured recently by *Datz et al.* [1995], and the reaction has been found to favor the production of three H atoms (channel (RC2)) by a factor of 3:1.

There are five possible channels in the dissociative recombination reaction of CH_5^+ (reactions (RC3)–(RC7)):

$$CH_5^+ + e \rightarrow CH_4 + H \quad (6)$$

$$\rightarrow CH_3 + H_2 \quad (7)$$

$$\rightarrow CH_3 + H + H \quad (8)$$

$$\rightarrow CH_2 + H_2 + H \quad (9)$$

$$\rightarrow CH + H_2 + H_2 \quad (10)$$

The cross sections and branching ratios have been measured in an ion storage ring at six different energies by *Semaniak et al.* [1998]. We have interpolated their branching ratios to a temperature of 200 K, and the results are shown in Table 3.

Recent experimental measurements have shown that recombination coefficients for hydrocarbon ions formed from a series of alkanes, alkenes, and alkynes do not increase with size for ions larger than about C_3- as one might expect, but level off at about $(7 - 8) \times 10^{-7}\,cm^3\,s^{-1}$ [*Lehfaoui et al.*, 1997; *Rebrion-Rowe et al.*, 1998]. Therefore we adopt here rate coefficients of $7.5 \times 10^{-7}\,cm^3\,s^{-1}$ for dissociative recombination of the ion classes $C_3H_n^+$ and $C_4H_n^+$.

Table 2. Selected Ion-Molecule Reactions

Number	Reactions	Rate Coefficient, $cm^3 s^{-1}$	Reference
R1	$H_2^+ + He \rightarrow HeH^+ + H$	0.	see text
R2	$H_3^+ + C_2H_6 \rightarrow C_2H_7^+ + H_2$	2.9×10^{-11}	
R3	$C^+ + CH_4 \rightarrow C_2H_2^+ + H_2$	3.64×10^{-10}	
R4	$\rightarrow C_2H_3^+ + H$	9.36×10^{-10}	
R5	$CH_3^+ + C_2H_4 \rightarrow C_2H_3^+ + CH_4$	4.88×10^{-10}	
R6	$\rightarrow C_3H_3^+ + H_2 + H_2$	4.24×10^{-11}	
R7	$\rightarrow C_3H_5^+ + H_2$	5.4×10^{-10}	
R8	$CH_4^+ + C_2H_4 \rightarrow C_2H_4^+ + CH_4$	1.7×10^{-9}	
R9	$\rightarrow C_2H_5^+ + CH_3$	2.6×10^{-10}	
R10	$\rightarrow C_3H_5^+ + H_2 + H$	6×10^{-11}	
R11	$CH_5^+ + H \rightarrow CH_4^+ + H_2$	$3.\times10^{-11}e^{-1460/T}$	see text
R12	$CH_5^+ + CH_4 \rightarrow$ products	3×10^{-11}	*McMahon et al.* [1976]
R13	$CH_5^+ + C_2H_6 \rightarrow C_2H_5^+ + CH_4 + H_2$	2.03×10^{-10}	
R14	$\rightarrow C_2H_7^+ + CH_4$	1.15×10^{-9}	
R15	$C_2H_2^+ + H_2 \rightarrow C_2H_3^+ + H$	$1.0\times10^{-10}e^{-800/T}$	see text
R16	$C_2H_2^+ + CH_4 \rightarrow C_3H_4^+ + H_2$	1.87×10^{-10}	
R17	$\rightarrow C_3H_5^+ + H$	7.0×10^{-10}	
R18	$C_2H_2^+ + C_2H_4 \rightarrow C_2H_4^+ + C_2H_2$	4.14×10^{-10}	
R19	$\rightarrow C_3H_3^+ + CH_3$	6.62×10^{-10}	
R20	$\rightarrow C_4H_5^+ + H$	3.17×10^{-10}	
R21	$C_2H_5^+ + CH_4 \rightarrow C_3H_7^+ + H_2$	9×10^{-14}	
R22	$C_2H_5^+ + C_2H_4 \rightarrow C_3H_5^+ + CH_4$	3.55×10^{-10}	
R23	$C_2H_5^+ + C_2H_6 \rightarrow C_3H_7^+ + CH_4$	5.5×10^{-12}	
R24	$\rightarrow C_4H_9^+ + H_2$	3.35×10^{-11}	
R25	$H_3^+ + CH_4 \rightarrow CH_5^+ + H_2$	2.4×10^{-9}	
R26	$CH_4^+ + H_2 \rightarrow CH_5^+ + H$	3×10^{-11}	*Federer et al.* [1985]
R27	$H^+ + CH_4 \rightarrow CH_3^+ + H_2$	3.69×10^{-9}	
R28	$H_2^+ + H_2 \rightarrow H_3^+ + H$	2×10^{-9}	*Clow and Futrell* [1972]
R29	$H^+ + H_2(v\geq4) \rightarrow H_2^+ + H$	2×10^{-9}	estimated
R30	$H_2^+ + CH_4 \rightarrow CH_5^+ + H$	1.1×10^{-10}	*Kim and Huntress* [1975]
R31	$C_2H_4^+ + C_2H_2 \rightarrow C_4H_5^+ + H$	2.37×10^{-10}	*Jarrold et al.* [1983]
R32	$He^+ + H_2 \rightarrow HeH^+ + H$	4.21×10^{-13}	*Schauer et al.* [1989]
R33	$\rightarrow H^+ + H + He$	8.8×10^{-14}	
R34	$H_2^+ + H \rightarrow H^+ + H_2$	6.4×10^{-10}	*Karpas et al.* [1979]
R35	$C_2H_4^+ + H \rightarrow C_2H_3^+ + H_2$	3×10^{-10}	*Hansel et al.* [1989]
R36	$C_2H_5^+ + H \rightarrow C_2H_4^+ + H_2$	1×10^{-11}	*Hansel et al.* [1989]
R37	$C_2H_3^+ + H \rightarrow C_2H_2^+ + H_2$	1×10^{-10}	*Hansel et al.* [1989]
R38	$HeH^+ + H \rightarrow H_2^+ + He$	9.1×10^{-10}	*Karpas et al.* [1979]

Only those reactions whose rate coefficients have been modified since the study of *Kim and Fox* [1994] and those necessary to the discussion are included. All rate coefficients, unless otherwise noted are from the evaluated compilation of *Anicich et al.* [1994].

We have included 39 neutral-neutral reactions for hydrocarbons up to C_2, and those reactions are shown in Table 4. This reaction set is admittedly smaller than the 194 reactions employed by *Gladstone et al.* [1996] in their model of the neutral hydrocarbon chemistry in the midlatitude thermosphere. A more complete neutral chemistry model would include the entire reaction set employed by Gladstone et al. but is outside the scope of this work.

3. The Model

3.1. Temperature Profile

We have constructed our standard model with information combined from Galileo and Voyager. The temperature profile we have adopted is a smoothed version of the profile derived from measurements of the Galileo Atmospheric Structure Instrument [*Seiff et al.*, 1997] and is shown in Figure 1. The original profile exhibits

Table 3. Selected Dissociative Recombination Reactions

Number	Reactions	Rate Coefficient, $cm^3 s^{-1}$	Reference
RC1	$H_3^+ + e \rightarrow H_2 + H$	$2.88\times10^{-8}(300/T_e)^{0.65}$	*Sundström et al.* [1994]
RC2	$\rightarrow H + H + H$	$8.63\times10^{-8}(300/T_e)^{0.65}$	*Datz et al.* [1995]
RC3	$CH_5^+ + e \rightarrow CH_2 + H_2 + H$	$5.3\times10^{-8}(300/T_e)^{0.52}$	*Semaniak et al.* [1998]
RC4	$\rightarrow CH_3 + H + H$	$1.9\times10^{-7}(300/T_e)^{0.52}$	
RC5	$\rightarrow CH_3 + H_2$	$1.7\times10^{-8}(300/T_e)^{0.52}$	
RC6	$\rightarrow CH_4 + H$	$9.0\times10^{-9}(300/T_e)^{0.52}$	
RC7	$\rightarrow CH + H_2 + H_2$	$9.5\times10^{-9}(300/T_e)^{0.52}$	
RC8	$C_2H^+ + e \rightarrow CH + C$	$6.5\times10^{-8}(300/T_e)^{0.5}$	*Mul and McGowan* [1980]
RC9	$C_2H_2^+ + e \rightarrow CH + CH$	$8.1\times10^{-8}(300/T_e)^{0.5}$	*Mul and McGowan* [1980]
RC10	$\rightarrow C_2H + H$	$1.9\times10^{-7}(300/T_e)^{0.5}$	
RC11	$C_2H_3^+ + e \rightarrow CH_2 + CH$	$2.3\times10^{-7}(300/T_e)^{0.5}$	*Mul and McGowan* [1980]
RC12	$\rightarrow C_2H_2 + H$	$2.3\times10^{-7}(300/T_e)^{0.5}$	
RC13	$C_2H_4^+ + e \rightarrow CH_2 + CH_2$	$1.75\times10^{-7}(300/T_e)^{0.5}$	estimate
RC14	$\rightarrow C_2H_3 + H$	$1.75\times10^{-7}(300/T_e)^{0.5}$	estimate
RC15	$C_2H_6^+ + e \rightarrow CH_4 + CH_2$	$3.5\times10^{-7}(300/T_e)^{0.5}$	estimate
RC16	$C_2H_7^+ + e \rightarrow C_2H_4 + H_2 + H$	$2.0\times10^{-7}(300/T_e)^{0.5}$	estimate
RC17	$\rightarrow C_2H_5 + H_2$	$2.0\times10^{-7}(300/T_e)^{0.5}$	estimate
RC18	$\rightarrow C_2H_6 + H$	$2.0\times10^{-7}(300/T_e)^{0.5}$	estimate
RC19	$C_3H_n^+ + e \rightarrow$ products	$7.5\times10^{-7}(300/T_e)^{0.5}$	estimate
RC20	$C_4H_n^+ + e \rightarrow$ products	$7.5\times10^{-7}(300/T_e)^{0.5}$	estimate
RC21	$H^+ + e \rightarrow H + h\nu$	$4\times10^{-12}(250/T_e)^{0.7}$	*Bates and Dalgarno* [1962]
RC22	$CH_3^+ + e \rightarrow CH_2 + H$	$3.5\times10^{-7}(300/T_e)^{0.5}$	*Mul et al.* [1981]

Only those reactions whose rate coefficients have been modified since the study of *Kim and Fox* [1994] and those necessary to the discussion are included.

a wavelike structure, with an exospheric temperature of about 900 K. The exospheric temperature derived from the Voyager solar occultation data was 1100 ± 200 K [*Atreya et al.*, 1981]. Although these values apply to nonauroral regions, we have assumed that the temperature profile applies to the auroral regions as well, to facilitate comparison with other calculations.

It is, however, likely that there are temperature differences between the auroral regions and lower latitudes. Precipitating electrons deposit 40–50% of their energy as heat [*Gérard and Singh*, 1982; *Waite et al.*, 1983], and therefore very large heating rates, of the order of a few ergs cm^{-2} s^{-1} or more, are implied by the observed ultraviolet intensities. Auroral temperatures from the stratosphere to the lower thermosphere (from about 100 mbar to 1 μbar) have been derived from ground-based and Voyager IRIS spectra of hydrocarbons and the values have been found to be significantly enhanced over those of nonauroral regions [e.g., *Kostiuk et al.* 1993; *Drossart et al.*, 1993b; *Livengood et al.*, 1993]. Temperatures in the middle auroral thermosphere have been inferred from the rotational structure in the infrared H_3^+ auroral emissions near the exobase and have been found to be higher than those at midlatitudes. *Drossart et al.* [1989] and *Drossart et al.* [1993a] derived rotational temperatures of 1000–1200 K and 1250±70 K, respectively, from Jovian auroral H_3^+ emission at 2 and 4 μm detected with the Canada-France-Hawaii Telescope. Observations of Jovian auroral H_3^+ emissions at 2.1 and 4.0 μm with the NASA Infrared Telescope facility at Mauna Kea indicated rotational temperatures of about 1100±100 K [*Miller et al.*, 1990]. It has been proposed that the heat deposited by the precipitating particles may be efficiently redistributed from the auroral zones to the equatorial regions by strong thermospheric winds [e.g., *Waite et al.*, 1983; *Emerich et al.*, 1996]. *Achilleos et al.* [1998] have constructed a three-dimensional dynamical model of the Jovian auroral ionosphere, in which auroral precipitation of 10 keV electrons with an energy flux of 8 ergs s^{-1} parallel to the local field lines produces outflowing winds of up to 35 m s^{-1} at the nanobar pressure level (just below 1000 km in our model) and 600 m s^{-1} at the upper boundary of their model. They noted that if the region of electron energy deposition is as narrow as recent HST images have shown it to be, the winds could be significantly stronger, but that modeling such wind speeds would require higher resolution than their current model allows.

The temperatures in the near-equatorial thermosphere of Jupiter have been derived from Voyager stellar occultation data, and values near 400 km were found to be about 200±50 K [*Atreya et al.*, 1981; *Festou et al.*, 1981]. Temperatures at the peak of auroral energy deposition have been inferred from analyses of the rota-

Table 4. Neutral-Neutral Reactions

Number	Reaction	Rate Coefficient, cm^3s^{-1}	Reference
RN1	$^1CH_2 + H \rightarrow CH + H_2$	5×10^{-11}	estimate
RN2	$^1CH_2 + H_2 \rightarrow {}^3CH_2 + H_2$	1.26×10^{-11}	*Braun et al.* [1970] *Langford et al.* [1983]
RN3	$\rightarrow CH_3 + H$	9.24×10^{-11}	*Braun et al.* [1970] *Langford et al.* [1983]
RN4	$^3CH_2 + H \rightarrow CH + H_2$	$1\times10^{-11}\exp(900/T)$	*Baulch et al.* [1992]
RN5	$^3CH_2 + {}^3CH_2 \rightarrow C_2H_2 + H + H$	$2.1\times10^{-10}\exp(-408/T)$	*Tsang and Hampson* [1986] *Frank et al.* [1986]
RN6	$CH_3 + H \rightarrow {}^1CH_2 + H_2$	$1\times10^{-10}\exp(-7600/T)$	*Baulch et al.* [1992]
RN7	$CH_3 + H_2 \rightarrow CH_4 + H$	$1.14\times10^{-20}T^{2.74}\exp(-4740/T)$	*Baulch et al.* [1992]
RN8	$CH_3 + {}^3CH_2 \rightarrow C_2H_4 + H$	$7.\times10^{-11}$	*Baulch et al.* [1992]
RN9	$CH_3 + CH_3 \rightarrow C_2H_5 + H$	$5\times10^{-11}\exp(-6800/T)$	*Baulch et al.* [1992]
RN10	$CH_4 + H \rightarrow CH_3 + H_2$	$2.18\times10^{-20}T^3\exp(-4045/T)$	*Baulch et al.* [1992]
RN11	$CH_4 + CH \rightarrow C_2H_4 + H$	$3\times10^{-11}\exp(200/T)$	*Berman and Lin* [1983] *Anderson et al.* [1987]
RN12	$CH_4 + {}^1CH_2 \rightarrow CH_4 + {}^3CH_2$	1.2×10^{-11}	*Böhland et al.* [1985]
RN13	$\rightarrow CH_3 + CH_3$	5.9×10^{-11}	*Böhland et al.* [1985]
RN14	$CH_4 + C_2H \rightarrow C_2H_2 + CH_3$	$9\times10^{-12}\exp(-250/T)$	*Allen et al.* [1992]
RN15	$C_2H + H_2 \rightarrow C_2H_2 + H$	$5.6\times10^{-11}\exp(-1443/T)$	*Stephens et al.* [1987]
RN16	$C_2H_2 + {}^3CH_2 \rightarrow C_3H_2 + H_2$	$1\times10^{-11}\exp(-3332/T)$	*Böhland et al.* [1985]
RN17	$\rightarrow C_3H_3 + H$	$1.\times10^{-11}\exp(-3332/T)$	*Böhland et al.* [1986]
RN18	$C_2H_2 + C_2H \rightarrow H + \text{products}$	1.5×10^{-10}	*Stephens et al.* [1987]
RN19	$C_2H_3 + H \rightarrow C_2H_2 + H_2$	2×10^{-11}	*Baulch et al.* [1992]
RN20	$C_2H_3 + H_2 \rightarrow C_2H_4 + H$	$2.6\times10^{-13}\exp(-2646/T)$	*Allen et al.* [1992]
RN21	$C_2H_3 + CH_3 \rightarrow C_2H_2 + CH_4$	6.5×10^{-13}	*Tsang and Hampson* [1986]
RN22	$C_2H_4 + H \rightarrow C_2H_3 + H_2$	$9\times10^{-10}\exp(-7500/T)$	*Baulch et al.* [1992]
RN23	$C_2H_4 + CH_3 \rightarrow C_2H_3 + CH_4$	$6.9\times10^{-12}\exp(-5600/T)$	*Baulch et al.* [1992]
RN24	$C_2H_5 + H \rightarrow C_2H_4 + H_2$	0.	*Baulch et al.* [1992]
RN25	$\rightarrow CH_3 + CH_3$	$6.\times10^{-11}$	*Tsang and Hampson* [1986]
RN26	$C_2H_5 + CH_3 \rightarrow C_2H_4 + CH_4$	$1.88\times10^{-12}(300/T)^{0.5}$	*Tsang and Hampson* [1986]
RN27	$C_2H_5 + C_2H_5 \rightarrow C_2H_6 + C_2H_4$	2.4×10^{-12}	*Baulch et al.* [1992]
RN28	$C_2H_6 + H \rightarrow C_2H_5 + H_2$	$2.35\times10^{-15}T^{1.5}\exp(-3725/T)$	*Baulch et al.* [1992]
RN29	$C_2H_6 + CH_3 \rightarrow C_2H_5 + CH_4$	$2.45\times10^{-31}T^6\exp(-3043/T)$	*Baulch et al.* [1992]
RN30	$H + H + H_2 \rightarrow H_2 + H_2$	$2.7\times10^{-31}T^{-0.6}$	*Baulch et al.* [1992]
RN31	$CH + H_2 + H_2 \rightarrow CH_3 + H_2$	$k_0 = 3.8\times10^{-29}\exp(-20/T)$ (T < 200 K)	*Laufer and Yung* [1983]
		$k_0 = 5.8\times10^{-30}\exp(355/T)$ (T > 200 K)	*Laufer and Yung* [1983]
		$k_\infty = 2.37\times10^{-12}\exp(523/T)$	*Berman and Lin* [1984]
RN32	$^3CH_2 + H + H_2 \rightarrow CH_3 + H_2$	$k_0 = 3.8\times10^{-29}\exp(-20/T)$ (T < 200 K)	*Gladstone et al.* [1996] (estimate)
		$k_0 = 5.8\times10^{-30}\exp(355/T)$ (T > 200)	*Gladstone et al.* [1996] (estimate)
		$k_\infty = 2.37\times10^{-12}\exp(523/T)$	*Gladstone et al.* [1996] (estimate)

Table 4. (continued)

Number	Reaction	Rate Coefficient, $cm^3 s^{-1}$	Reference
RN33	$CH_3 + H + H_2 \rightarrow CH_4 + H_2$	$k_0 = 5.44\times10^{-22}T^{-1.8}$	*Cobos and Troe* [1990]
		$k_\infty = 2.0\times10^{-9}T^{-0.4}$	*Tsang* [1989]
RN34	$CH_3 + CH_3 + H_2 \rightarrow C_2H_6 + H_2$	$k_0 = 3.5\times10^{-7}T^{-7}\exp(-1390/T)$	*Baulch et al.* [1992]
		$k_\infty = 6\times10^{-11}$	*Baulch et al.* [1992]
RN35	$CH_3 + C_2H_5 + H_2 \rightarrow C_3H_8 + H_2$	$k_0 = 1.01\times10^{-22}\exp(341/T)$ (T < 200 K)	*Laufer and Yung* [1983]
		$k_0 = 2.22\times10^{-26}\exp(2026/T)$ (T > 200 K)	*Tsang and Hampson* [1986]
		$k_\infty = 8.1\times10^{-10}T^{-0.5}$	*Tsang and Hampson* [1986]
RN36	$C_2H_2 + H + H_2 \rightarrow C_2H_3 + H$	$k_0 = 3.3\times10^{-30}\exp(-740/T)$	*Baulch et al.* [1992]
		$k_\infty = 1.4\times10^{-11}\exp(-1300/T)$	*Baulch et al.* [1992]
RN37	$C_2H_4 + H + H_2 \rightarrow C_2H_5 + H_2$	$k_0 = 2.15\times10^{-29}\exp(-349/T)$	*Lightfoot and Pilling* [1987]
		$k_\infty = 4.39\times10^{-11}\exp(-1087/T)$	*Allen et al.* [1992]
RN38	$C_2H_5 + H + H_2 \rightarrow C_2H_6 + H_2$	$k_0 = 5.5\times10^{-23}T^{-2}\exp(-1040/T)$	*Teng and Jones* [1972]
		$k_\infty = 1.5\times10^{-10}$	*Munk et al.* [1986]
RN39	$C_2H_6 + C_2H \rightarrow C_2H_5 + C_2H_2$	6×10^{-12}	*Baulch et al.* [1992]

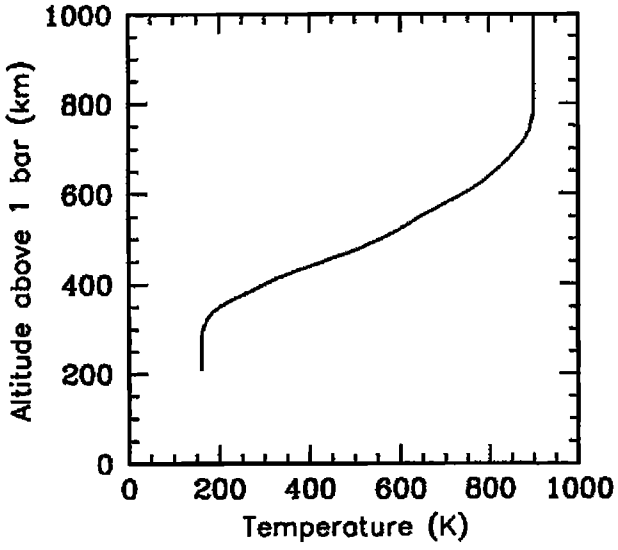

Figure 1. Smoothed temperature profile from the Galileo Atmospheric Structure Instrument [*Seiff et al.*, 1997].

tional structure of the H_2 bands in spectra obtained with the HST GHRS. These spectra are assumed to arise mainly from the altitude of maximum emission, which coincides approximately with the altitude of maximum electron energy deposition. *Trafton et al.* [1994] analyzed HST spectra of the Lyman and Werner bands of H_2 in the 1252–1288 and 1572–1607 Å ranges, and reported temperatures of 530±100 K. *Clarke et al.* [1994] analyzed spectra of the northern auroral regions in the wavelength range 1204–1241 Å and derived temperatures of 400–700 K. *Kim et al.* [1995] reported temperatures of 200–800 K from spectra in the wavelength range 1586–1620 Å; from the spectra that exhibited the brightest H_2 bands, temperatures of 200-500 K were derived.

Liu and Dalgarno [1996] reanalyzed these HST spectra using more recent wavelengths and transition probabilities for the Lyman and Werner band systems from *Abgrall et al.* [1993a,b] and including the effect of secondary electrons. They derived temperatures of 300–700 K, with values of 400–500 K for the brightest auroral regions. In 1995, *Kim et al.* [1997] obtained six additional spectral pairs of Lyman and Werner band emissions and analyzed these spectra and those from their 1993 observations [*Kim et al.*, 1995] with updated molecular data and including the effect of secondary electrons. They derived temperatures in the range 300–850 K, with a value of 450 K for the brightest spectrum.

The precipitating electrons have been found in previous studies to deposit most of their energy in the region of or just below the hydrocarbon homopause, which is near 440 km above the 1-bar level for the midlatitude model from Voyager [*Atreya et al.*, 1981]. In our standard (Galileo) model the homopause is at about 375 km, which is significantly lower than in the Voyager model.

Here we use our model of electron energy deposition in the auroral regions to compare the temperatures at the altitudes of peak energy deposition using the Galileo temperature profile to those derived from HST spectra.

3.2. Eddy Diffusion Coefficient

Because of the large energy input by precipitating particles, mixing processes in the auroral regions may be much more efficient than those in the midlatitude thermosphere. *Kim et al.* [1997] presented a plot of temperature inferred from their HST Jovian auroral spectra versus pressure for several models. They found that the temperature-pressure pairs would fit the Galileo model fairly well if an admittedly unrealistic model with a constant mixing ratio of methane throughout the thermosphere were assumed. This model would be consistent with a very large auroral eddy diffusion coefficient and a very high homopause. Here we have constructed three models that differ mainly in the eddy diffusion profile assumed. In our standard model (A), the eddy diffusion coefficient in $cm^2\,s^{-1}$ is given by

$$K = A\left(\frac{1.4\times10^{13}}{n_t}\right)^{1/2} \tag{11}$$

where n_t is the total number density in cm^{-3} and $A = 1.4\times10^6$ was derived by *Atreya et al.* [1981] (see also *Festou et al.* [1981]) by fitting model H_2 and CH_4 density profiles to Voyager data: the H_2 density at a methane optical depth of unity at Lyman alpha derived from the stellar occultation data, and the tropopause mixing ratio implied by the Voyager IRIS data [*Hanel et al.*, 1979]. The methane density profile in our model is completely determined by our choice of the Voyager value for A, and the Galileo value for the methane mixing ratio at the lower boundary of the model (200 km). We note here that the methane mixing ratio in our model at 5 μbar is about 5×10^{-4} and not the value 2.5×10^{-5} derived from the Voyager stellar occultation data. In order to reproduce that mixing ratio, we would have to reduce the value of A considerably. It is unlikely that the effective eddy diffusion coefficient in the auroral thermosphere is less than that at midlatitudes, although it is possible that eddy diffusion does not adequately represent the vertical mixing produced by the actual wind field in the auroral regions. Strong auroral winds have been derived in the dynamical 3-D model of *Achilleos et al.* [1998].

For models B and C, we have increased the values for A by factors of 3 and 10, respectively. As the eddy diffusion coefficient increases, the altitude of the homopause also rises, and the resulting values of the eddy diffusion coefficients at the homopauses are 1.8×10^6, 1×10^7, and 8×10^7 $cm^2\,s^{-1}$, for models A, B, and C, respectively. The altitude of the homopause rises from 375 to 505 km, and the temperature increases from about 250 to 570 K from model A to model C. The homopause characteristics of the three models are compared in Table 5.

3.3. Background Density Profiles

Background density profiles for H_2, He, H, CH_4, C_2H_2, C_2H_4, and C_2H_6 for the standard and enhanced eddy diffusion coefficient models are shown in Figures 2a–2c. The neutral density profiles in the three models were computed including both molecular and eddy diffusion. The H_2 density profiles were constructed by setting the total pressure at 200 km to that derived from measurements of the Galileo probe [*Seiff et al.*, 1997]. The densities at higher altitudes were then determined using the temperature profile and the eddy diffusion coefficients described in section 3.2. The helium mixing ratio, defined here as the fraction by number or volume, at the lower boundary was assumed to be 0.135, as determined by *Niemann et al.* [1996] from the Galileo probe mass spectrometer, and by *Von Zahn and Hunten* [1996] from the Galileo Helium Abundance Detector.

The H_2 densities derived from Galileo data at and above 200 km are smaller than those derived from Voyager data. For example, at 200 km the H_2 density in our model A is $7.8\times10^{15}\,cm^{-3}$, whereas in the Voyager model the density is $1\times10^{16}\,cm^{-3}$. The difference at 400 km is larger: 3.8×10^{12} cm^{-3} in the Galileo model and 2×10^{13} cm^{-3} in the Voyager model. This reflects the slightly lower mesospheric temperatures measured by the Galileo Atmospheric Structure Experiment [*Seiff et al.*, 1997] compared those interpolated from the Voyager IRIS and radio science measurements [*Festou et al.*, 1981].

Table 5. Homopause Characteristics of Models A, B, and C

	A	B	C
Altitude, km	375	425	505
K_h, cm^2s^{-1}	1.8×10^6	9.9×10^6	7.6×10^7
Pressure, μbar	0.283	8.93×10^{-3}	2.70×10^{-3}
Temperature, K	247	361	567
H_2 density, cm^{-3}	7.95×10^{12}	1.70×10^{12}	3.22×10^{11}
H_2 column density, cm^{-2}	3.37×10^{19}	1.05×10^{19}	3.13×10^{18}
CH_4 density, cm^{-3}	2.16×10^7	1.54×10^7	6.14×10^6
CH_4 column density, cm^{-2}	1.88×10^{13}	1.97×10^{13}	1.28×10^{13}

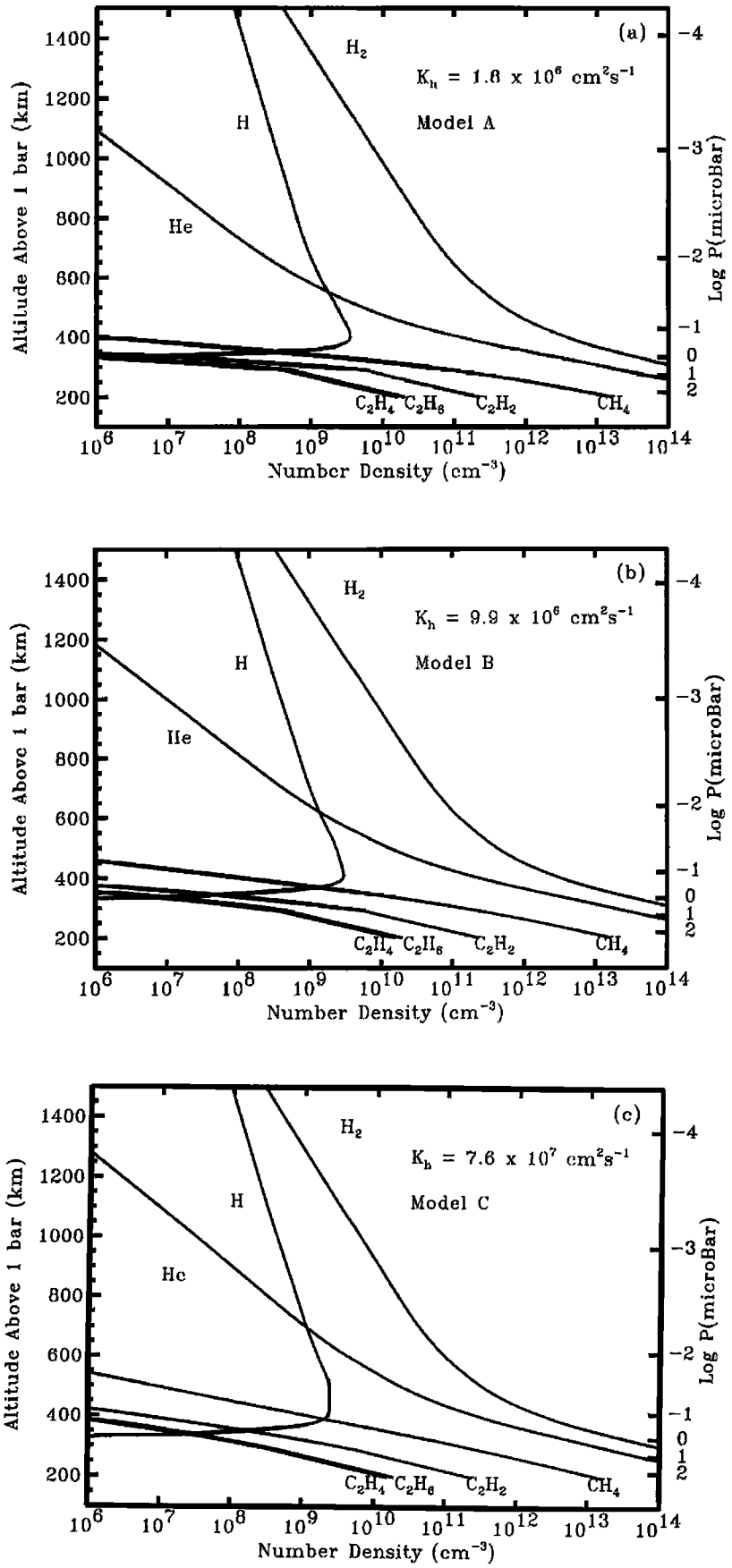

Figure 2. Density profiles of the background atmosphere for (a) model A, (b) model B, and (c) model C. The altitudes on the left vertical axis are referred to the 1 bar level. The right axis gives the pressure level.

For our models the density profiles for the long-lived stable hydrocarbons CH_4, C_2H_2, C_2H_4, and C_2H_6 were determined with the assumption that chemistry does not affect their densities. The mixing ratio of methane at the bottom of the model was assumed to be 2.1×10^{-3}, as measured by the Galileo probe mass spectrometer [*Niemann et al.*, 1996]. The C_2H_6 mixing ratio was assumed to be 2×10^{-6} at the 5 μbar level, as Voyager stellar occultation measurements indicated [*Atreya et al.*, 1981; *Festou et al.*, 1981]. For C_2H_2 and C_2H_4 the mixing ratios determined in the calculations of *Gladstone et al.* [1996] were fixed at their peak values of 3×10^{-5} and 2×10^{-6}, respectively, at the 4 μbar level, near 300 km, and assumed constant below that altitude. In our models B and C with increased eddy diffusion coefficients, the high-altitude hydrocarbon densities are enhanced relative to those in the standard model.

The assumption that precipitation and subsequent chemistry does not affect the densities of the major stable neutral hydrocarbons in the auroral regions is certainly not strictly correct. Indeed, all the C_2 hydrocarbons are ultimately produced from methane photochemically. The detailed neutral hydrocarbon model of *Gladstone et al.* [1996] shows that the C_2H_2, C_2H_4, and C_2H_6 mixing ratios peak near 4–5 μbar, and that the densities may be reduced at lower altitudes either by increasing the supply of H from higher altitudes or by increasing the eddy diffusion coefficient. Both effects may be produced by auroral particle precipitation. The auroral effects in our calculations are, however, concentrated near and above 300 km, and our results are not much affected by the assumptions about the density profiles of the C_2 hydrocarbons below this altitude.

Further evidence about variations of neutral hydrocarbon densities from the auroral zones to lower latitudes is reflected in infrared emissions, some of which have been observed to be enhanced in the auroral regions, and some of which are reduced. For example, *Drossart et al.* [1986] measured enhanced acetylene emission at 13.3 μm from the north pole of Jupiter using the NASA Infrared Telescope Facility. *Caldwell et al.* [1980] observed enhanced emissions from methane in the ν_4 fundamental from the Jovian polar regions at 7.8 μm. Using infrared heterodyne spectroscopy at 12 mm, *Kostiuk et al.* [1989], however, found no evidence for increased emission from ethane near 60°N latitude, and one set of measurements showed an actual decrease. Such variations in infrared emissions may arise from variations in temperature or in the abundances of the emitting species, either of which may occur in the auroral regions.

Coupling of auroral precipitation and neutral chemistry is also indicated by the existence of auroral hazes [*Pryor and Hord*, 1991]. The ion chemistry, which is coupled to the neutral chemistry, may play some role in haze production as well. These issues are important and will be taken into account in future models in which the neutral chemistry is more complete than that which we have adopted here.

Another important but ill-defined factor for the chemistry of the auroral ionosphere is the size of the auroral regions and the rate of horizontal transport both into and out of the region. This transport may be rapid and may greatly affect the number densities of species with long chemical lifetimes. The latitudinal extent of the intense auroral precipitation is uncertain. The stated intensity of auroral emissions (in kR) depends on the assumed width of the oval. Initially, the oval was assumed to be about 6000 km wide because that is the width of the magnetic projection of the edges of the Io torus onto the planet, and the precipitating particles were assumed to originate from the torus [*Sandel et al.*, 1979]. The identification of the primary particles as heavy ions has been shown to be improbable over the last few years, and HST FUV images have also shown the emitting region to be significantly narrower than previously supposed, sometimes of the order of only hundreds of kilometers [*Gérard et al.*, 1994; *Clarke et al.*, 1996]. Furthermore, diffuse emissions are observed poleward of the narrow, bright arc [*Gérard et al.*, 1994; *Ballester et al.*, 1996]. A multidimensional calculation would be necessary to model these effects. Our assumption that the density profiles of methane and the three stable C_2 hydrocarbons are not affected by precipitation or chemistry is equivalent to assuming that horizontal transport is rapid enough to reduce their density gradients. This is, however, a significant source of uncertainty in our model.

Evidence concerning the atomic hydrogen density profiles in the auroral regions is conflicting. In the nonauroral regions the major source of dayglow Lyman alpha is resonance scattering of the solar line, and therefore the measured intensity is indicative of the column abundance of H above the methane absorption altitude. An atomic H column density of about $1 \times 10^{17}\,\mathrm{cm}^{-2}$ above the methane absorption altitude was inferred from the Voyager Lyman alpha airglow data by *McConnell et al.* [1980]. From a disk-averaged Lyman alpha intensity of 13 kR measured with a sounding rocket, *Clarke et al.* [1980] derived a global average H atom layer of 3.2×10^{17} cm^{-2}. Similar average intensities of about 10 kR were reported for the Lyman alpha dayglow outside the "bulge" region from IUE spectra [*Skinner et al.*, 1983; see also *Skinner et al.*, 1988]. *Skinner et al.* [1988] analyzed IUE observations of Jovian dayglow Lyman alpha over the 8-year period 1978–1986 and concluded that, since the intensities tracked that of the solar Lyman alpha line fairly closely, the column density of H had remained essentially unchanged over that period at about $10^{17}\,\mathrm{cm}^{-2}$, as determined earlier by *Gladstone* [1982a,b]. Recently, *Ben Jaffel et al.* [1993] used a sophisticated radiative transfer code to model the Jovian bulge and nonbulge Lyman alpha intensities measured by IUE and found

that a column density of about $3.7 \times 10^{17}\,cm^{-2}$ reproduced the nonbulge data well.

Waite et al. [1983] computed the H density profile for the solar EUV source alone and found that, for their standard eddy diffusion coefficient, the atomic hydrogen profile was characterized by a peak density of $1.3 \times 10^{10}\,cm^{-3}$ near 400 km and a column-integrated density of $1.75 \times 10^{17}\,cm^{-2}$ above the methane absorbing layer. The standard eddy diffusion coefficient used by Waite et al. (about 1×10^{6} $cm^2\,s^{-1}$ at the homopause) was determined by fitting the density profiles of methane and ethane to the Voyager stellar occultation data [*Atreya et al.*, 1981] and is similar to our K value for model A. Smaller H column densities, of the order of $10^{16}\,cm^{-2}$, were obtained only for homopause eddy diffusion coefficients in excess of about $10^{7}\,cm^2\,s^{-1}$. Waite et al. also computed the average H density profile that would result if H produced in the auroral regions were distributed uniformly over the globe (by, for example, thermospheric winds) and predicted a column abundance of about 6×10^{17} cm^{-2}.

Recently, *Prangé et al.* [1997] have derived H column densities from an analysis of the shape of the auroral Lyman alpha line obtained at high spectral resolution with the GHRS on HST. The auroral Lyman alpha emission is produced mainly by dissociative excitation of H_2 by the precipitating electrons, although on the dayside there is also a significant component due to resonance scattering of solar radiation. The line profile exhibits a strong central reversal, which occurs due to resonance scattering of the emitted photons by a population of H atoms above the emitting region. Thus the line shape may be exploited to determine the column abundance of H atoms above the region of production or the methane absorption altitude. The auroral column densities inferred by Prangé et al., $(1-5) \times 10^{16}$ H atoms cm^{-2}, are smaller even than the midlatitude values inferred from the Lyman alpha dayglow observations.

For our background models, we have fixed the column density of H at $1 \times 10^{17}\,cm^{-2}$ above the homopause, as a compromise between the equatorial and midlatitude column abundances inferred from measurements and models and the values derived by *Prangé et al.* [1997] for the auroral region. We then predict the steady state atomic hydrogen density profile implied by our precipitation calculation. While the computed auroral atomic hydrogen densities may be reduced by transport from the polar to the equatorial regions, thermospheric winds are unlikely to decrease the H column densities in the polar region to values smaller than those at midlatitudes. It is possible, however, that the smaller auroral atomic hydrogen column densities are a consequence of stronger vertical mixing, which enhances the high-altitude densities of species that react with H and also transports H atoms to lower altitudes, where they are destroyed more efficiently. We therefore explore here the effect of increasing the eddy diffusion coefficient on the H density profiles.

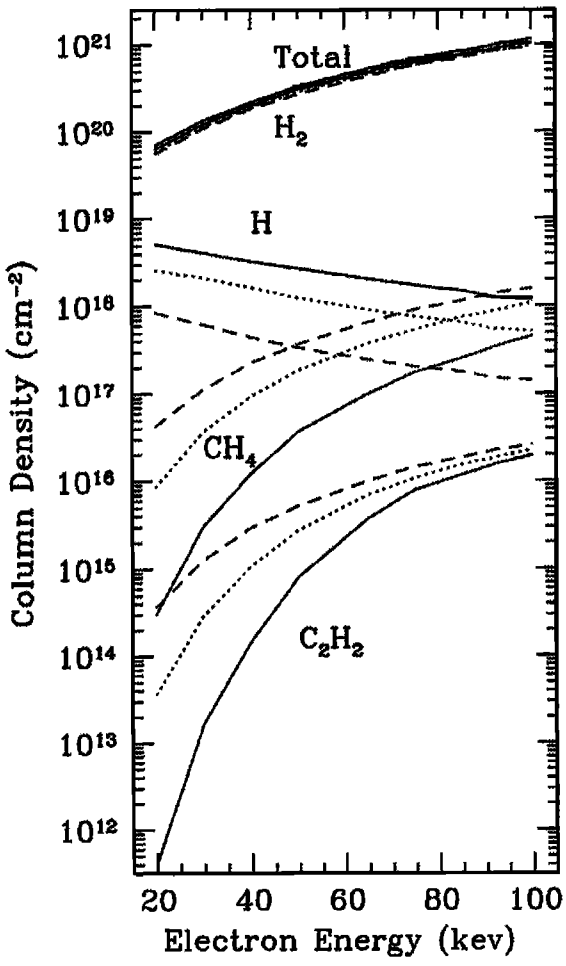

Figure 3. Column densities above the electron energy deposition peak as a function of energy of the precipitating primary electron. Models A, B, and C are shown as solid, dotted, and dashed lines, respectively. For H the column densities are above the methane $\tau = 1$ level at Lyman alpha (1216 Å), if that altitude is above the energy deposition peak.

4. Results

The column densities of H_2, H, CH_4, and C_2H_2 to which the precipitating electrons are predicted to penetrate as a function of electron energy from 20 to 100 keV for each of the three models are presented in Figure 3. The H_2 column densities are not significantly model-dependent; the values vary from about 6×10^{19} to $10^{21}\,cm^{-2}$ as the electron energy increases from 20 keV to 100 keV. Recently, *Wolven and Feldman* [1998] analyzed auroral spectra of the Lyman and Werner bands obtained with HUT. The transitions in the wavelength region below 1100 Å terminate on low vibrational levels of H_2, and the degree of observed self-absorption indicates the vibrational temperature and depth from which the emissions originate. From the measured intensities of emissions terminating on $v = 2$, Wolven and Feldman derived H_2 vertical column densities of $1.5 \times 10^{20}\,cm^{-2}$. For our models this corresponds to an electron energy of about 30 keV.

The methane column densities above the altitude of peak electron energy deposition for the standard model increase from $3 \times 10^{14}\,cm^{-2}$ to $4 \times 10^{17}\,cm^{-2}$ over the electron energy range considered here. These values are considerably smaller than those computed by *Singhal et al.* [1992] because the abundance of methane in our model atmosphere is significantly smaller than theirs. As expected, the column densities of hydrocarbons, including methane, are larger for the enhanced eddy diffusion coefficients. The average methane column densities inferred from IUE and HST spectra are of the order of $(3-6) \times 10^{16}\,cm^{-2}$. As Figure 3 shows, those column densities correspond to energies of 45–55 keV for the standard model atmosphere. For models B and C, with enhanced eddy diffusion, the corresponding energies are 25–30 keV and about 15–20 keV, respectively. By comparison, *Gladstone and Skinner* [1989] inferred an electron energy of about 95 keV, and *Singhal et al.* [1992] derived a value of 30 keV. The sources of the difference are not easy to identify, since the model atmospheres used in those studies were different, and the electron transport was handled in very different ways from ours. *Waite et al.* [1983] carried out a two-stream electron transport calculation that should give comparable results to ours, but their inferred electron energies of 1–10 keV reflected the then prevalent belief that the electrons did not penetrate to below the methane homopause. *Waite et al.* [1988] analyzed two spectra of the Jovian auroral regions measured by IUE and determined penetration depths by modifying laboratory spectra by the hydrocarbon transmission curves of *Yung et al.* [1982]. They reported that precipitating electrons with energies in the 10–30 keV range were most likely, with a best fit of 22.5 keV.

We have also determined the acetylene column densities to which the electrons penetrate as a function of electron energy for the three models, and the results are also shown in Figure 3. C_2H_2 column densities of $(4-12)\times10^{14}$, $(1-3)\times10^{14}$, and $(2-4)\times10^{14}\,cm^{-2}$ are predicted for models A, B, and C, respectively, for the precipitating electron energies derived from the measured methane column densities. Our acetylene column

Table 6a. Column Production Rates of Selected H Sources for Model B with 30 keV Precipitating Electrons

Number	Reaction	Column Production Rate, $cm^{-2}s^{-1}$
RN3	$^1CH_2 + H_2 \rightarrow CH_3 + H$	1.59×10^{10}
RN11	$CH + CH_4 \rightarrow C_2H_4 + H$	2.10×10^{10}
RN15	$C_2H + H_2 \rightarrow C_2H_2 + H$	3.47×10^{9}
RN18	$C_2H + C_2H_2 \rightarrow H +$ products	2.15×10^{9}
RN20	$C_2H_3 + H_2 \rightarrow C_2H_4 + H$	1.64×10^{8}
RC1	$H_3^+ + e \rightarrow H_2 + H$	3.61×10^{9}
RC2	$H_3^+ + e \rightarrow H + H + H$	3.24×10^{10}
RC3	$CH_5^+ + e \rightarrow CH_2 + H + H_2$	7.84×10^{9}
RC4	$\rightarrow CH_3 + H + H$	5.71×10^{10}
RC6	$\rightarrow CH_4 + H$	1.33×10^{9}
RC10	$C_2H_2^+ + e \rightarrow C_2H + H$	1.50×10^{8}
RC12	$C_2H_3^+ + e \rightarrow C_2H_2 + H$	4.36×10^{8}
RC18	$C_2H_7^+ + e \rightarrow C_2H_6 + H$	1.77×10^{8}
RC21	$H^+ + e \rightarrow H + h\nu$	1.52×10^{8}
RC22	$CH_3^+ + e \rightarrow {}^1CH_2 + H$	4.45×10^{8}
R15	$C_2H_2^+ + H_2 \rightarrow C_2H_3^+ + H$	1.93×10^{11}
R17	$C_2H_2^+ + CH_4 \rightarrow C_3H_5^+ + H$	2.21×10^{10}
R26	$CH_4^+ + H_2 \rightarrow CH_5^+ + H$	1.05×10^{10}
R27	$H^+ + CH_4 \rightarrow CH_4^+ + H$	1.87×10^{9}
R28	$H_2^+ + H_2 \rightarrow H_3^+ + H$	1.78×10^{11}
R31	$C_2H_4^+ + C_2H_2 \rightarrow C_4H_5^+ + H$	9.07×10^{6}
R32	$He^+ + H_2 \rightarrow HeH^+ + H$	2.97×10^{9}
R33	$\rightarrow H^+ + H + He$	6.20×10^{8}
	$CH_4 + h\nu \rightarrow {}^3CH_2 + H + H$	7.66×10^{9}
	$\rightarrow CH + H + H_2$	6.01×10^{8}
	$C_2H_2 + h\nu \rightarrow C_2H^* + H$	1.18×10^{7}
	$\rightarrow C_2H + H$	3.58×10^{9}
	$C_2H_4 + h\nu \rightarrow C_2H_2 + H + H$	1.06×10^{10}
	$C_2H_6 + h\nu \rightarrow C_2H_4 + H + H$	7.33×10^{6}
	$H_2 + e^* \rightarrow H^+ + H + 2e$	7.01×10^{9}
	$\rightarrow H + H + e$	1.68×10^{11}

Table 6b. Column Loss Rates of H for the Major H Sinks for Model B with 30 keV Precipitating Electrons

Number	Reaction	Column Loss Rate, $cm^{-2}s^{-1}$
RN1	$^1CH_2 + H \rightarrow CH + H_2$	1.24×10^{8}
RN4	$^3CH_2 + H \rightarrow CH + H_2$	1.97×10^{10}
RN10	$CH_4 + H \rightarrow CH_3 + H_2$	1.29×10^{8}
RN19	$C_2H_3 + H \rightarrow C_2H_2 + H_2$	7.80×10^{9}
RN22	$C_2H_4 + H \rightarrow C_2H_3 + H_2$	5.06×10^{1}
RN25	$C_2H_5 + H \rightarrow CH_3 + CH_3$	3.77×10^{10}
RN30	$H + H + H_2 \rightarrow H_2 + H_2$	2.78×10^{11}
RN33	$CH_3 + H + H_2 \rightarrow CH_4 + H_2$	1.19×10^{11}
RN36	$C_2H_2 + H + H_2 \rightarrow C_2H_3 + H_2$	8.12×10^{9}
RN37	$C_2H_4 + H + H_2 \rightarrow C_2H_5 + H_2$	3.78×10^{10}
RN38	$C_2H_5 + H + H_2 \rightarrow C_2H_6 + H_2$	1.05×10^{6}
R11	$CH_5^+ + H \rightarrow CH_4 + H_2$	8.38×10^{9}
R34	$H_2^+ + H \rightarrow H^+ + H_2$	1.05×10^{9}
R41	$HeH^+ + H \rightarrow H_2^+ + He$	2.73×10^{7}
R43	$C_2H_3^+ + H \rightarrow C_2H_2^+ + H_2$	2.22×10^{11}
R35	$C_2H_4^+ + H \rightarrow C_2H_3^+ + H_2$	1.24×10^{10}
R36	$C_2H_5^+ + H \rightarrow C_2H_4^+ + H_2$	1.19×10^{10}
	$H + h\nu \rightarrow H^+ + e$	2.23×10^{9}
	$H + e^* \rightarrow H^+ + 2e$	6.67×10^{7}

densities are smaller than those of methane by about a factor of 50, in rough agreement with the broad range of 10–100 derived by *Ajello et al.* [1998] from Galileo UVS spectra. It should be noted, however, that the acetylene column densities are strongly model-dependent, and there is significant uncertainty in the abundance of acetylene at thermospheric altitudes both in the auroral regions and at lower latitudes.

The atomic hydrogen production rates in the auroral regions are greatly enhanced over those arising from the interaction of solar EUV fluxes with H_2 at lower latitudes. The major sources of H in the auroral regions, along with column integrated production or loss rates, are listed in Table 6a. Altitude profiles of the most important production mechanisms of H for 30 keV electrons precipitating into our model B are shown in Figure 4. At altitudes above about 450 km, the major sources are dissociative recombination of H_3^+ (reactions (RC1) and (RC2)) and the reaction of H_2^+ with H_2 (reaction (R28)). The altitude profile of reaction (R28) resembles the electron-impact ionization profile. Other important sources of H include direct electron-impact dissociation of H_2,

$$H_2 + e^* \rightarrow H + H, \qquad (12)$$

dissociative recombination of CH_5^+ (RC3, RC4, and RC6), and the slightly endothermic ion-molecule reaction (R15)

$$C_2H_2^+ + H_2 \rightarrow C_2H_3^+ + H. \qquad (13)$$

The column integrated rate of this reaction is large more because it involves the dominant neutral H_2 than because the density of $C_2H_2^+$ is large. In fact, the most important C_2 ions are $C_2H_5^+$ and $C_2H_3^+$, and the most important source of $C_2H_2^+$ is the exothermic reverse reaction (R37), which we will discuss below. Other important sources of $C_2H_2^+$ include the reaction of C_2H^+ with H_2 and charge transfer from H_2^+ and He^+ to C_2H_2. Direct production of $C_2H_2^+$ by photoionization and auroral electron impact ionization of C_2H_2 is also significant.

As the model eddy diffusion coefficient increases, the altitude range over which reaction (R15) dominates becomes larger, and the altitude at which H_3^+ dissociative recombination (reactions (RC1) and (RC2)) exceeds reaction (R15) rises. For the C_2H_4 profile that we have adopted, photodissociation of ethylene

$$C_2H_4 + h\nu \rightarrow C_2H_2 + 2H \qquad (14)$$

dominates the production of H below about 300 km.

The major chemical sinks of atomic hydrogen for 30 keV electrons precipitating into thermospheric model B are listed, along with integrated column loss rates, in Table 6b, and altitude profiles are shown in Figure 5. The reaction of H with $C_2H_3^+$ (reaction (R37))

$$C_2H_3^+ + H \rightarrow C_2H_2^+ + H_2 \qquad (15)$$

is the dominant destruction mechanism for H in the 340 to 470 km region. The reverse of reaction (R37) (reaction (R15)), which we have discussed above, is an important source of H, and its rate is nearly as large as that of (R37). Thus the sequence of reactions (R37) followed by (R15) constitutes a "null cycle" that mit-

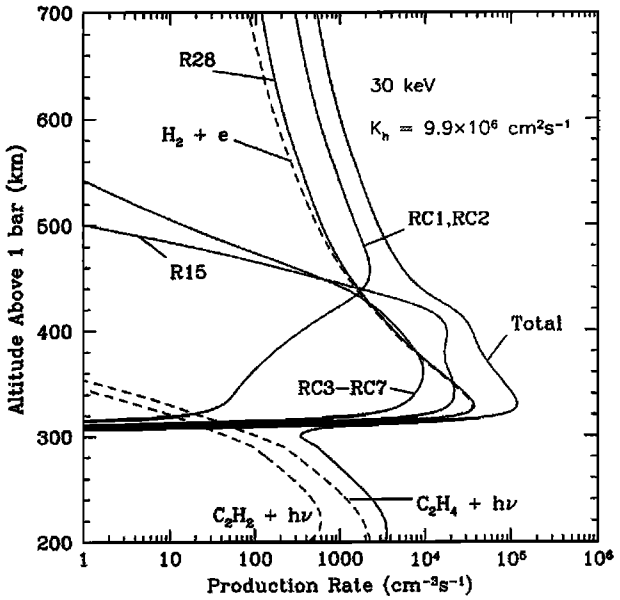

Figure 4. Altitude profiles of the most important atomic hydrogen production rates for model B with 30 keV precipitating electrons. The dashed curve is production due to electron impact dissociation of H_2. The solid curves are ion-molecule reactions and dissociative recombination reactions. The curves are labeled with the numbers of the reactions in Tables 1, 2, and 3. The curve labeled "Total" is the sum of all production processes.

igates the effect of either reaction on the H chemistry. The sink of H in reaction (R37) exceeds the source in reaction (R15) only by about 10%, for a net column loss rate of about $2 \times 10^{10}\,\mathrm{cm}^{-2}\,\mathrm{s}^{-1}$. The reactions of H with $C_2H_4^+$ (R35) and with $C_2H_5^+$ (R36) are also important but are not shown in Figure 5. Their profiles peak near 330 km, with rates of about 2000 $\mathrm{cm}^{-3}\,\mathrm{s}^{-1}$.

The three-body recombination reactions (RN33)

$$\mathrm{CH_3 + H + M \rightarrow CH_4 + M}, \tag{16}$$

and (RN37)

$$\mathrm{C_2H_4 + H + M \rightarrow C_2H_5 + M}, \tag{17}$$

and the bimolecular reaction (RN25)

$$\mathrm{C_2H_5 + H \rightarrow CH_3 + CH_3}, \tag{18}$$

however, are the most important loss process for H below about 300 km. The three-body reaction (RN30) of H with itself

$$\mathrm{H + H + M \rightarrow H_2 + M} \tag{19}$$

dominates the destruction of H from about 300 to 340 km.

Other important H destruction mechanisms include reaction (RN1) with $^1CH_2$ and reaction (RN4) with $^3CH_2$. The sequence of reaction (RN19)

$$\mathrm{C_2H_3 + H \rightarrow C_2H_2 + H_2} \tag{20}$$

followed by the three-body reaction (RN36)

$$\mathrm{C_2H_2 + H + M \rightarrow C_2H_3 + M} \tag{21}$$

makes up a catalytic cycle for recombination of H to form H_2 [e.g., *Gladstone et al.*, 1996] but is significant only on the bottomside of the H layer. The three-body loss processes were identified as important by previous investigators [e.g., *Waite et al.*, 1983; *Atreya et al.*, 1981; *Gladstone et al.*, 1996], but the ion-molecule reactions were not.

For model B with 30 keV electron precipitation, the figures show that photochemical equilibrium (PCE) is a valid approximation for H only up to about 250 km. Above that altitude, auroral production of H is balanced by downward transport to altitudes where it is destroyed by three-body chemical reactions. The numerical value of the downward flux of H at 400 km in model B is about 1×10^{11} cm^{-2} s^{-1} and is equal to the net production rate of H above that altitude. If the precipitating electron energies are larger, the H atoms are produced lower in the atmosphere, and production and loss are more nearly balanced at the altitude of peak production.

For a given atmospheric model, as the energy of the precipitating electrons increases, the maximum in the H production rate profile shifts to lower altitudes, and

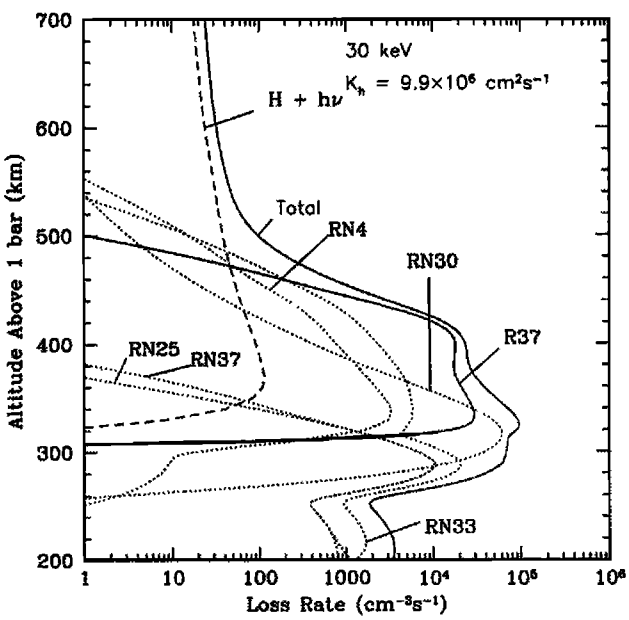

Figure 5. Altitude profiles of the most important atomic hydrogen loss rates for model B with 30 keV precipitating electrons. The dashed curves are processes involving the interaction of photons or energetic electrons with neutrals; the solid curves are ion-molecule reactions and recombinations; the dotted curves are neutral-neutral reactions. The curves are labeled with the numbers of the reactions in Tables 1, 2 and 3. The curve labeled "Total" is the sum of all loss processes.

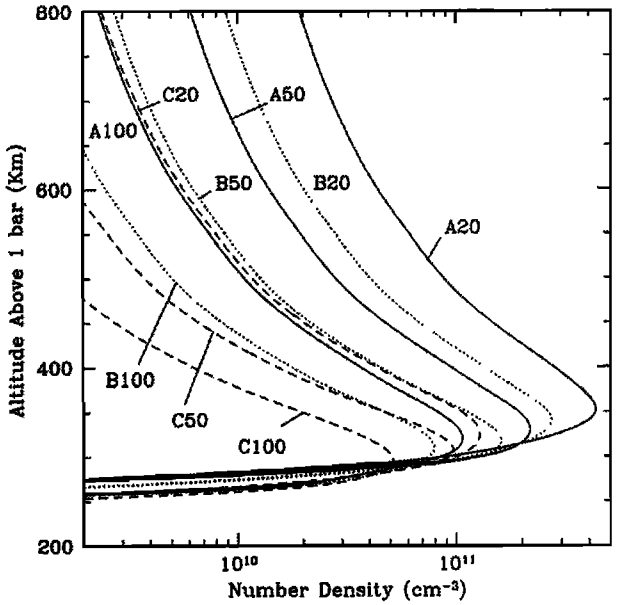

Figure 6. Atomic hydrogen density profiles. Models A, B, and C are shown as solid, dotted, and dashed curves, respectively. The curves are labeled with the letter of the model followed by the energy (in keV) of the primary electron. For example, A50 denotes model A with 50 keV precipitating electrons.

the three-body recombination reactions become more important relative to the ion-molecule reactions as loss processes for H. For a given energy of the precipitating electrons, as the eddy diffusion coefficient increases, the three-body recombination of two H atoms (reaction (RN30)) becomes less important at high altitudes, and the reactions of H with methane and with hydrocarbon ions become more important.

The computed density profiles of atomic hydrogen for all three models at the precipitation energies of 20, 50, and 100 keV are presented in Figure 6. The altitude of the peak density is in the range 300–350 km for all models. For a given model the peak densities decrease monotonically with energy of the precipitating electrons, and for a given electron energy the densities decrease with increasing eddy diffusion coefficient. For example, for 50 keV electrons the peak densities of atomic H are 2×10^{11}, 1.5×10^{11}, and 1×10^{11} cm^{-3} for models A, B, and C, respectively. For model B, the peak H densities are 2.7×10^{11}, 1.6×10^{11}, and 8×10^{10} cm^{-3} for 20, 50, and 100 keV electrons. Our computed H density profiles are similar to those presented by *Waite et al.* [1983], but their computed H peak and column integrated densities are greater for 10 keV electrons than for 1 keV electrons. Waite et al. explained this trend as due to the decreased production of atomic H by low-energy electrons, which deposit their energy at higher altitudes, where the ratio of H to H_2 is larger. Although our models exhibit the opposite behavior (increasing H densities with decreasing electron energy), our calculations differ from those of Waite et al. because our background models, by design, all contain nearly the same H profile for all energies of precipitating electrons. Also, we did not construct models for precipitating electron energies as low as 1–10 keV. It is quite possible that the predicted H densities do not vary monotonically with electron energy at low energies. It is only at very low energies that the electrons deposit their energy high enough in the thermosphere for the H densities to be significant for the electron energy loss. Indeed, Waite et al. estimated an H density profile for 125 keV electron precipitation in which the peak was lower and the peak density smaller than that produced by precipitation of either 1 or 10 keV electrons.

The computed atomic hydrogen column densities presented in Figure 3 are integrated above either the altitude of peak electron energy deposition or the methane absorption altitude, whichever is higher. These are the column densities that would be inferred from auroral Lyman alpha intensity data. The methane absorption altitude is that for which the column density is equal to about 5×10^{16} cm^{-2}, the inverse of the CH_4 photoabsorption cross section at Lyman alpha (2×10^{-17} cm^2). The methane absorption altitude is higher than the peak of the electron energy deposition only for the highest energy electrons and the highest eddy diffusion coefficients. For our standard model the H column decreases from about 6×10^{18} cm^{-2} for 20 keV electrons to 1×10^{18} cm^{-2} for 100 keV electrons. For the atmospheres with enhanced eddy diffusion coefficients, the computed H columns are smaller. For model C the variation is from 1×10^{18} cm^{-2} for 20 keV electrons

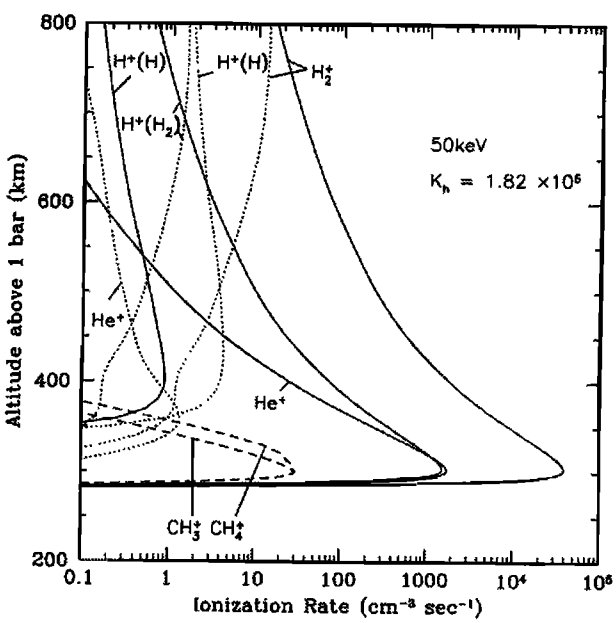

Figure 7. Selected altitude profiles of the direct ionization rates for model A with 50 keV precipitating electrons. The solid curves are electron-impact processes; the dotted curves are photoionization and photodissociative ionization; the dashed curves are the sum of electron-impact and photoionization.

Table 7. Column Ionization Rates for Models A, B and C at Three Energies

Parent		Model A			Model B			Model C		
Neutral	Channel	20 keV	50 keV	100 keV	20 keV	50 keV	100 keV	20 keV	50 keV	100 keV
H_2	H_2^+	1.81×10^{11}	1.70×10^{11}	1.72×10^{11}	1.80×10^{11}	1.75×10^{11}	1.72×10^{11}	1.81×10^{11}	1.70×10^{11}	1.72×10^{11}
	H^+	7.17×10^{9}	6.74×10^{9}	6.84×10^{9}	7.16×10^{9}	6.94×10^{9}	6.82×10^{9}	7.17×10^{9}	6.74×10^{9}	6.83×10^{9}
H	H^+	1.26×10^{8}	2.38×10^{7}	6.59×10^{6}	1.34×10^{8}	2.58×10^{7}	6.84×10^{6}	1.41×10^{8}	2.60×10^{7}	7.00×10^{6}
He	He^+	3.54×10^{9}	6.12×10^{9}	8.14×10^{9}	6.87×10^{9}	9.02×10^{9}	9.94×10^{9}	9.83×10^{9}	1.04×10^{10}	1.08×10^{10}
CH_4	CH_4^+	4.09×10^{6}	6.12×10^{7}	2.25×10^{8}	8.24×10^{7}	3.07×10^{8}	5.10×10^{8}	3.57×10^{8}	5.88×10^{8}	7.31×10^{8}
	CH_3^+	3.61×10^{6}	5.84×10^{7}	1.99×10^{8}	7.27×10^{7}	2.71×10^{8}	4.50×10^{8}	3.15×10^{8}	5.19×10^{8}	6.46×10^{8}
	CH_2^+	5.34×10^{5}	8.28×10^{6}	2.93×10^{7}	1.08×10^{7}	4.00×10^{7}	6.65×10^{7}	4.66×10^{7}	7.67×10^{7}	9.54×10^{6}
	CH^+	1.73×10^{5}	2.79×10^{6}	9.49×10^{6}	3.48×10^{6}	1.29×10^{7}	2.15×10^{7}	1.51×10^{7}	2.48×10^{7}	3.09×10^{7}
	C^+	8.71×10^{4}	1.41×10^{6}	4.79×10^{6}	1.75×10^{6}	6.52×10^{6}	1.09×10^{7}	7.60×10^{6}	1.25×10^{7}	1.56×10^{7}
	H^+	2.64×10^{5}	4.27×10^{6}	1.45×10^{7}	5.32×10^{6}	1.98×10^{7}	3.29×10^{7}	2.31×10^{7}	3.80×10^{7}	4.72×10^{7}
C_2H_2	$C_2H_2^+$	2.05×10^{4}	3.38×10^{6}	1.40×10^{7}	7.80×10^{5}	8.29×10^{6}	1.65×10^{7}	5.64×10^{6}	1.38×10^{7}	1.89×10^{7}
	C_2H^+	4.07×10^{3}	6.70×10^{5}	2.77×10^{6}	1.55×10^{5}	1.64×10^{6}	3.26×10^{6}	1.12×10^{6}	2.75×10^{6}	3.75×10^{6}
	C_2^+	1.14×10^{3}	1.87×10^{5}	7.74×10^{5}	4.31×10^{4}	4.58×10^{5}	9.10×10^{5}	3.12×10^{5}	7.68×10^{5}	1.05×10^{6}
	CH^+	1.12×10^{3}	1.85×10^{5}	7.66×10^{5}	4.27×10^{4}	4.53×10^{5}	9.00×10^{5}	3.08×10^{5}	7.60×10^{5}	1.03×10^{6}
	C^+	5.03×10^{2}	8.29×10^{4}	3.43×10^{5}	1.91×10^{4}	2.03×10^{5}	4.03×10^{5}	1.38×10^{5}	3.40×10^{5}	4.63×10^{5}
C_2H_4	all ions	2.75×10^{2}	7.27×10^{4}	3.45×10^{5}	1.25×10^{4}	1.71×10^{5}	3.73×10^{5}	1.02×10^{5}	2.90×10^{5}	4.16×10^{5}
C_2H_6	all ions	1.41×10^{3}	4.81×10^{5}	2.28×10^{6}	7.95×10^{4}	1.15×10^{6}	2.46×10^{6}	6.95×10^{5}	1.92×10^{6}	2.69×10^{6}
Total	Ionization	1.92×10^{11}	1.83×10^{11}	1.87×10^{11}	1.94×10^{11}	1.92×10^{11}	1.90×10^{11}	1.99×10^{11}	1.88×10^{11}	1.91×10^{11}

Rates are in units of $cm^{-2}s^{-1}$

to $1.3 \times 10^{17}\,cm^{-2}$ for 100 keV electrons. The atomic hydrogen column densities are less as the electron energy increases because the H atoms are produced lower in the atmosphere, where they may be destroyed efficiently by reaction with hydrocarbons. For a given electron energy, as the eddy diffusion coefficient increases, the hydrocarbon neutral and ion densities increase at high altitudes, so the atomic hydrogen loss rates increase at higher altitudes. Our computed H densities are, of course, maximum values, since our model does not include transport of H out of the auroral regions by thermospheric winds. It is, however, noteworthy that the computed H column densities are not reduced to values that are less than those at lower latitudes or to those that were derived by *Prangé et al.* [1997] from the auroral Lyman alpha line shape, at least for the most probable combinations of eddy diffusion coefficients and electron energies that we find. Although the predicted H columns are small, about $10^{17}\,cm^{-2}$, for the highest electron energies and model C, the corresponding methane column densities above the altitude of peak absorption are about $10^{18}\,cm^{-2}$ and are much too large for this combination to be probable.

Although we have plotted in Figure 3 the column densities of H that would be derived from Lyman alpha data, this is not necessarily equal to the total column density of H in the model. For model A, and 50 keV electrons, the total H column is about 2.9×10^{18} $cm^{-2}\ s^{-1}$, which is close to that shown in Figure 3. For model B, with 30 keV electrons, and model C, with 20 keV electrons, the total H column densities are about 2.8×10^{18} and 1.59×10^{18} cm^{-2}, respectively. Both of these values are larger than the column densities in Figure 3, mostly because the methane densities are enhanced at higher altitudes in the higher eddy diffusion models, and thus unit optical depth occurs at higher altitudes.

4.1. Ion Density Profiles

The production rates of ions for our standard model and an electron energy of 50 keV are presented in Figure 7. The peak of ion production occurs near the peak of electron energy deposition, near 300 km. The major ions produced are H_2^+, H^+, He^+, CH_4^+, and CH_3^+. As expected, the altitude of the peak in the H_2^+ production profile decreases with increasing energy of the precipitating electrons but, for a given electron energy, is not much affected by changes in the eddy diffusion coefficient. Integrated column ionization rates for all of our models for 20, 50 and 100 keV electrons are presented in Table 7. The integrated H_2^+ production rates are nearly the same for all of our models, largely because the energy fluxes were normalized to that necessary to produce 60 kR of Lyman band emission, and the shape of the H_2 electron-impact ionization cross section is similar to that for excitation of the B state of H_2. The production rate of hydrocarbon ions, however, increases significantly with both electron energy and eddy diffusion coefficient. Direct production of hydrocarbon ions

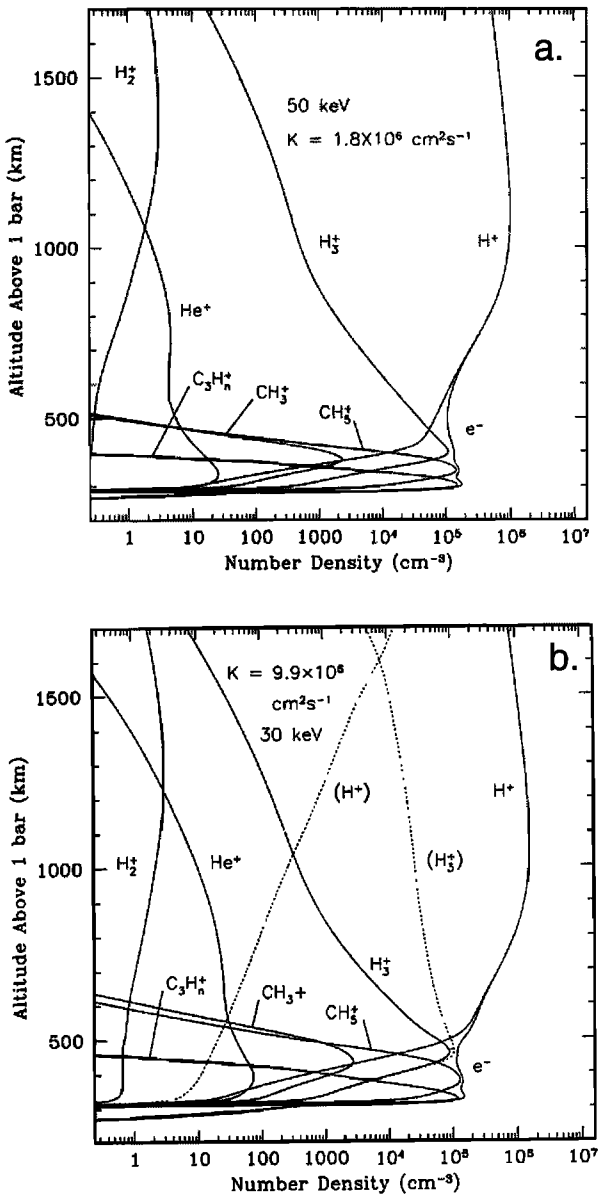

Figure 8. Computed density profiles for selected ions for (a) model A with 50 keV precipitating electrons, and (b) model B with 30 keV precipitating electrons. The dotted curves are the density profiles for H^+ and H_3^+ for an enhanced H_2 vibrational temperature of 4000 K.

by electron impact is, however, small compared to production via ion-molecule reactions, as we will discuss below.

The major ions that are produced are transformed by ion-molecule reactions; the steady state ion densities are shown in Figure 8a for model A, with 50 keV precipitating electrons, and in Figure 8b for model B, with 30 keV precipitating electrons. Even though H_2^+ is the major ion produced, it is transformed by reaction with H_2 into H_3^+ (reaction(R28)). H^+ is the major ion above about 450 km. Modeling the topside Jovian radio occultation profiles has generally been problematic, with predicted electron density peaks generally larger and lower in altitude than the observed values at middle or equatorial latitudes. H^+ is destroyed slowly by radiative recombination and more efficiently by charge transfer to vibrationally excited H_2 (reaction(R29))

$$H^+ + H_2(v \geq 4) \rightarrow H_2^+ + H \qquad (22)$$

if H_2 is sufficiently vibrationally excited [*McElroy*, 1973]. In solar source only (nonauroral) models without reaction (R29) above, the altitude of the peak electron density is near 600 km, and the peak density is in excess of $10^6\,cm^{-3}$ or more [e.g., *Waite et al.*, 1983; *Atreya et al.*, 1979]. Radio occultation profiles showed that the peak densities at midlatitudes occur higher in the atmosphere, at altitudes of 1000 to 2000 km, and are an order of magnitude smaller than the model values [*Eshleman et al.*, 1979a,b; *Hinson et al.*, 1998].

Enhanced and sometimes altitude-variable H_2 vibrational temperatures and/or vertical ion drifts have been successfully invoked to reproduce the observed midlatitude electron density peaks [e.g., *Waite et al.*, 1983; *Majeed and McConnell*, 1991]. *Cravens* [1987] carried out the first model calculation of the vibrational distribution of H_2 in the auroral and nonauroral thermospheres and showed that, with the computed vibrational populations, the solar-only model electron densities were reduced by the required factor of 10 at high altitudes, but the peak electron density was about $4 \times 10^5\,cm^{-3}$ at an altitude of about 600 km. *Majeed et al.* [1991] computed the vibrational distribution of H_2 in the nonauroral Jovian thermosphere, including fluorescence in the Lyman and Werner bands, which *Cravens* [1987] had neglected. The electron density profiles that they computed were similar to those of Cravens but could not be made to fit the existing midlatitude radio occultation profiles, even with vertical drifts imposed.

The Voyager 2 entrance radio science electron density profile at 65°S latitude was near the auroral zone, although until recently, only the topside electron densities had been derived for this occultation. A recent reanalysis of the Voyager 2 radio science entrance data shows an electron density peak near 650 km of about 3.5×10^5 cm^{-3} [*Hinson et al.*, 1998]. This altitude is close to that predicted by auroral models without reaction (R29) or vertical drifts, but the measured electron peak density (about $(3-4) \times 10^5\,cm^{-3}$) is smaller than model peak densities by 2 orders of magnitude [e.g., *Waite et al.*, 1983; *Singhal et al.*, 1992]. Waite et al. managed to match the high-altitude measurements with an altitude variable H_2 vibrational temperature, but the peak was still too high, at about 1000 km. For the auroral case with 10 keV electron precipitation, including the computed H_2 vibrational distribution and reduced H densities, *Cravens* [1987] found the auroral electron density peak was reduced by a factor of 10 but was still greater than $1 \times 10^6\,cm^{-3}$.

Perhaps coincidently, the solar source model electron density profiles of *Cravens* [1987] and *Majeed et al.* [1991] seem to fit the measured Voyager 2 entrance (66°S latitude) profile derived by *Hinson et al.* [1998] remarkably well. The auroral ion production rates are, however, larger than those at midlatitudes, leading to model electron densities that are 2 orders of magnitude greater than the Voyager 2 entrance profile [*Hinson et al.*, 1998]. Hinson et al. suggest that the photochemical models fit because the tangent point of the occultation was near but not in the auroral zone. Whether this is true, or whether the larger auroral production can be cancelled out with a reasonable auroral vibrational distribution of H_2 or vertical drifts, is unknown and probably will remain so until more is understood about the auroral thermosphere compared to the nonauroral thermosphere. The vibrational temperature of H_2 in the auroral regions may be enhanced because the rate of production of vibrationally excited H_2 by electron impact is larger and because the emission rates in the H_2 bands are enhanced. If, however the H densities are larger than at midlatitudes, the rate of quenching will also be higher [e.g., *Cravens*, 1987].

We have chosen to sidestep these questions here. For reaction (R29) we have assumed a constant vibrational temperature of 1470 K, which yields an effective rate coefficient of 1×10^{-15} cm^{3}s^{-1}. As Figures 8a and 8b show, the model H^+ peak density is near 1000 km, with a value of about $(2-3) \times 10^6$ cm^{-3}. We have also computed ion density profiles for a higher H_2 vibrational temperature of 4000 K, and the resulting H^+ profile is shown also as a dashed curve in Figure 8b. For this high vibrational temperature, H_3^+ is the dominant ion over a large altitude range, and the H^+ peak rises to an altitude of 1960 km. It is noteworthy that in this case, the Jovian ionosphere exhibits an extensive F_1 (molecular ion) peak. Thus we find, as have others, that increasing the vibrational temperature of H_2 decreases the H^+ peak density, but the F_2 peak also rises to altitudes much higher than observed. A model with a more realistic H_2 vibrational distribution, in which the degree of vibrational excitation increases with altitude, could probably be constructed to fit the data but would not further our understanding of the Jovian auroral ionosphere. Instead, we focus here on the lower ionosphere, which has been less explored.

In a narrow altitude range near 400 km in our standard model, the H_3^+ density exceeds that of H^+, with a peak density of about $(1-2) \times 10^5$ cm^{-3}, which decreases as the electron energy increases. The total column density of H_3^+ in our standard model A for 50 keV precipitating electrons is about 1.2×10^{12} cm^{-2} (Figure 8a); for model B with 30 keV electrons it is similar, about 1.1×10^{12} cm^{-2} (Figure 8b); for model C with 20 keV electron precipitation the H_3^+ column is slightly less, 9.5×10^{11} cm^{-2}. These values can be compared to those derived from measured intensities of the H_3^+ ν_2 fundamental and overtone transitions at 4 and 2 μm. Our column densities are on the low end of the range inferred by *Drossart et al.* [1989] of $(1.1-11) \times 10^{12}$ cm^{-2} and in the middle of the range inferred by *Drossart et al.* [1993a] of $(6-19) \times 10^{11}$ cm^{-2}. We note, however, that the use of a higher H_2 vibrational temperature increases the column density of H_3^+. Indeed, if we increase the vibrational temperature of H_2 to 4000 K, as shown in Figure 8b for model B, the H_3^+ column density increases to about 4×10^{12} cm^{-2}, which is larger than can be accommodated by the observations of *Drossart et al.* [1993a].

Below about 400 km, hydrocarbon ions become dominant, and the total density peak is also of the order of $(1-2) \times 10^5$ cm^{-3}. In the enhanced eddy diffusion coefficient models the altitude where hydrocarbon ions dominate is shifted to higher altitudes, and the hydrocarbon ion layer broadens. The most important hydrocarbon ion over about a 50 km range below the H_3^+ peak is CH_5^+, which is produced by reaction of CH_4^+ with H_2 (reaction (R26)) and by reaction of H_3^+ with CH_4 (reaction (R25)). Above the CH_5^+ layer, the most important hydrocarbon ion is CH_3^+, which is produced by the reaction of H^+ with CH_4 (reaction (R27)). At lower altitudes C_1 and C_2 ions are transformed to higher hydrocarbon ions, and the class of C_3 and C_4 ions become more important. The hydrocarbon ion density profiles are similar in shape and composition to those predicted by *Kim and Fox* [1994] for midlatitudes at local noon, but the predicted peak densities are an order of magnitude greater for the auroral ionosphere than for the nonauroral ionosphere.

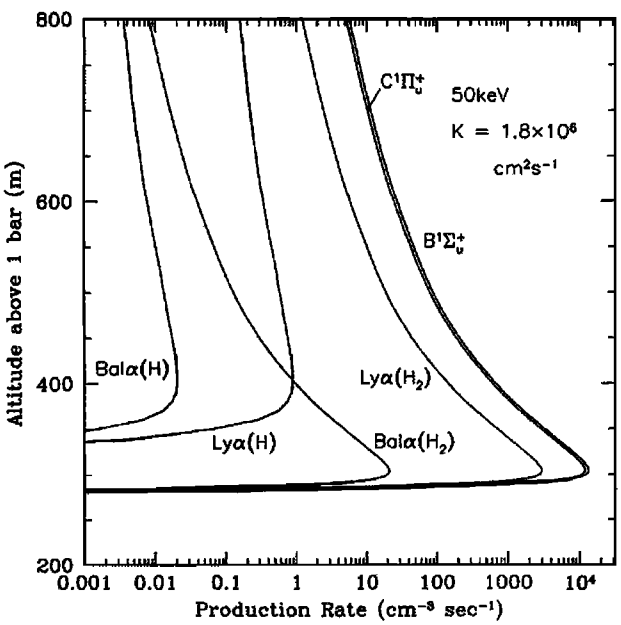

Figure 9. Altitude profiles of computed excitation rates for various excited states or emission of H_2 and H. The species in parentheses are the parent species. The curves labeled Lyα and Balα are emission rates of H Lyman alpha and H Balmer alpha. The curves labeled $C^1\Pi_u^+$ and $B^1\Sigma_u^+$ are production rates of the excited states of H_2.

The total densities of the hydrocarbon ions that we predict are similar to those computed by *Singhal et al* [1992]. Their predicted peak hydrocarbon ion densities are of the order of $10^5\,cm^{-3}$. There are differences in the compositional details, however, that may relate to the neutral background model atmosphere, the "polar model" proposed by *Livengood et al.* [1990], that they use. For example, H_3^+ does not dominate anywhere in their model. Although *Waite et al.* [1983] computed density profiles for six hydrocarbon ions in their comprehensive model, individual ion density profiles were not presented, so no detailed comparison is possible. Their electron density profiles do not show any structure on the bottomside that would signify a hydrocarbon ion layer, but the energies of the precipitating electrons adopted by Waite et al., 1 and 10 keV, were chosen to avoid penetrating far into the methane layer. The lack of a hydrocarbon ion layer is therefore not surprising. The chemistry of the lower ionosphere will be examined in detail in a later publication.

The recent reanalysis of the Voyager 2 entrance radio occultation by *Hinson et al.* [1998] has shown that the electron densities exceed $1 \times 10^5\,cm^{-3}$ below the main peak at 640 km down to about 420 km. Our models exhibit significant ionization down to about 300 km. The difference may relate to the background atmosphere that we have adopted, which is essentially for the equatorial regions, or as Hinson et al. have suggested, the Voyager 2 entrance profile may be near but not in the auroral zone.

4.2. Excitation and Emission Rates

Precipitation of energetic electrons in the polar regions produces emissions of H_2 in the Lyman ($B^1\Sigma_u^+ \rightarrow X^1\Sigma_g^+$) and Werner ($C^1\Pi_u \rightarrow X^1\Sigma_g^+$) band systems, H Lyman alpha, and H Balmer alpha, among others. Production rate profiles for some of the excited states of H_2 and H are presented in Figure 9. The excitation rates peak near 300 km in our models, with values of $1 \times 10^4\ cm^{-3}s^{-1}$ for both the H_2 B and C states. Integrated excitation rates are presented in Table 8. The estimated column excitation rates for the B and C states are about $60 \times 10^9\,cm^{-2}\,s^{-1}$, and $54 \times 10^9\,cm^{-2}\,s^{-1}$ for all the models. Cascading from the E/F states to the B state will increase the emission in the Lyman bands by about 15%. The energy fluxes of the precipitating electrons were determined by the requirement that the intensity of Lyman band emission be about 60 kR before absorption by CH_4. The emergent intensities will be modified by hydrocarbon absorption at wavelengths shortward of the thresholds, which are at about 1450 Å

Table 8. Column Production Rates for Model B at Three Energies

Channel	20 keV	50 keV	100 keV
B $^1\Sigma_u^+$	6.0×10^4	6.0×10^4	6.0×10^4
B′ $^1\Sigma_u^+$	1.0×10^4	1.0×10^4	1.0×10^4
B″ $^1\Sigma_u^+$	1.5×10^3	1.3×10^3	1.2×10^3
C $^1\Pi_u$	5.4×10^4	5.4×10^4	5.4×10^4
D $^1\Pi_u$	9.1×10^3	8.7×10^3	8.6×10^3
D′ $^1\Pi_u$	3.8×10^3	3.4×10^3	3.2×10^3
E,F $^1\Sigma_g^+$	9.0×10^3	8.8×10^3	8.7×10^3
Lyman-α (H_2)	1.0×10^4	9.2×10^3	8.8×10^3
Balmer-α (H_2)	1.4×10^3	1.4×10^3	1.3×10^3
Balmer-β (H_2)	2.2×10^2	2.1×10^2	2.0×10^2
Balmer-γ (H_2)	5.6×10^1	5.2×10^1	4.9×10^1
Lyman-α (H)	1.31×10^2	2.58×10^1	6.91
Balmer-α (H)	2.19×10^1	4.29	1.15

Rates are in units of $10^6\ cm^{-2}s^{-1}$

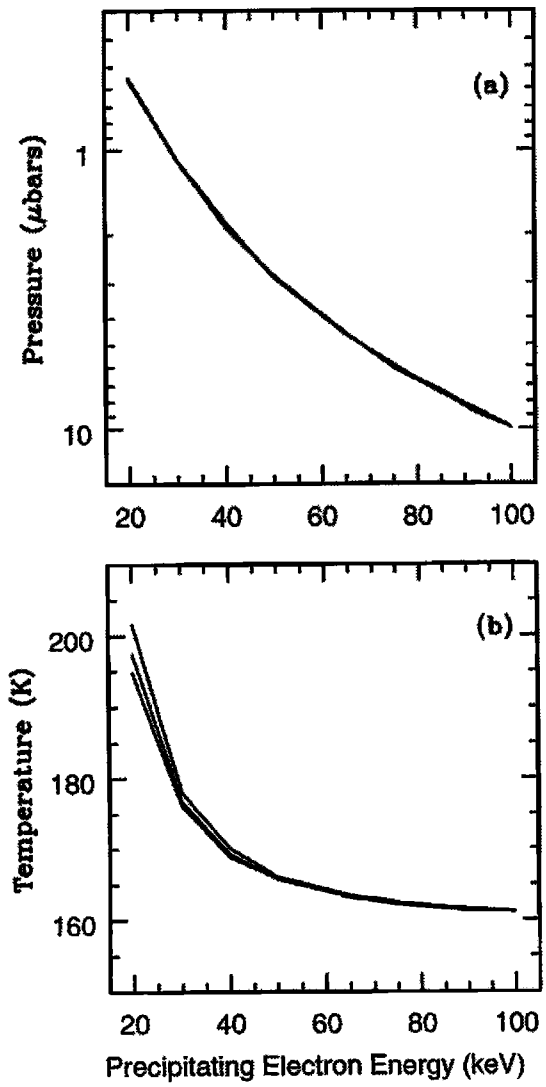

Figure 10. (a) Atmospheric temperature at the altitude of peak electron energy deposition as a function of primary electron energy for models A, B, and C. Low-energy primaries deposit their energy slightly lower in the atmosphere for the high eddy diffusion coefficient models than the low eddy diffusion coefficient models. (b) Pressure at the altitude of peak electron energy deposition.

for CH_4 and 1850 Å for C_2H_2. The H_2 emission bands terminating on low vibrational levels ($v \leq 2$) are optically thick [*Wolven and Feldman*, 1998]. The bands are reabsorbed, and their intensity is distributed among the other bands, so a detailed radiative transfer calculation may not be needed to determine the emission rates. We will model the predicted H_2 spectra in a later publication.

The integrated total production rate of H($2p$), the upper state of the Lyman alpha line, is $(13 - 14) \times 10^9$ cm^{-2} s^{-1} and is produced mainly by electron-impact dissociative excitation of H_2. Resonance scattering of solar radiation should also make a significant contribution to the auroral Lyman alpha intensity on the dayside. Determining the resonance scattering component and the emergent intensity of Lyman alpha emission would require a radiative transfer calculation, such as has been carried out by *Gladstone* [1982b], *Ben Jaffel et al.* [1993], and *Prangé et al.* [1997].

The computed integrated intensity of the Balmer alpha and beta lines, which arises mainly from electron-impact dissociative excitation of H_2, is 1.5–1.6 kR. The total auroral overhead intensity in the visible has been estimated by *Cook et al.* [1981] from Voyager images as 5 kR. Significantly larger values were inferred by *Ingersoll et al.* [1998] but for a much narrower auroral oval.

4.3. Temperatures and Pressures at the Auroral Energy Deposition Peak

We present in Figures 10a and 10b the pressure and temperature at the altitude of peak energy deposition as a function of energy of the precipitating electrons for all our models. No significant differences were seen for models A, B, and C, which differ mainly in the expressions for the eddy diffusion coefficient and thus mainly in the hydrocarbon density profiles. The H_2 profiles change only slightly from one model to another. The pressure at the electron energy deposition peak increases from about 0.5 to 10 μbar, and the temperature at the peak decreases from 200 to 160 K as the energy of the primary electrons increases from 20 to 100 keV. These temperatures are much lower than those inferred from rotational analyses of high-resolution spectra of the H_2 Lyman and Werner band systems, which are in the range 300 to 850 K at the peak of the emitting layer, with most values near 400–500 K [*Trafton et al.*, 1994; *Clarke et al.*, 1994; *Liu and Dalgarno*, 1996; *Kim et al.*, 1997]. This provides another piece of evidence that the auroral thermosphere is considerably warmer than the equatorial or midlatitude thermosphere.

5. Summary and Conclusions

We have modeled the Jovian auroral thermosphere and ionosphere by carrying out multistream electron transport calculations for a standard model thermosphere (model A) based on Galileo pressure and temperature profiles. The altitude profiles of methane and the stable C_2 hydrocarbons in our standard model A were designed to be consistent with the Galileo atmospheric structure experiment [*Seiff et al.*, 1997] and the calculations of *Gladstone et al.* [1996]. The expression for the eddy diffusion coefficient K in the standard model is that derived from the Voyager stellar occultation data [*Festou et al.*, 1981; *Atreya et al.*, 1981]. In addition, we have carried out calculations for two additional models in which the homopause values for K are factors of about 5.5 and 40 greater than the standard value.

The precipitating electrons were assumed to be essentially monoenergetic with nine energies in the range 20–100 keV, and the fluxes were assumed to be isotropic over the downward hemisphere. Energy fluxes of about 11 ergs cm^{-2}s^{-1} were chosen to produce 60 kR of Lyman band emission, approximately the average value inferred by *Kim et al.* [1997] from HST data. This energy flux is only slightly larger than that employed in previous models by *Waite et al.* [1983] and *Singhal et al.* [1992]. From our calculations, we have derived column densities of H_2, H, CH_4, and C_2H_2 above the peak of the energy deposition profile of the precipitating electrons. The methane column densities inferred from recent spectral modeling of the Lyman and Werner band system are mostly in the range $(2 - 7) \times 10^{16}$ cm^{-2} [*Waite et al.*, 1988; *Gladstone and Skinner*, 1989; *Trafton et al.*, 1994; *Kim et al.*, 1997; *Morrissey et al.*, 1997]. From these values, we can infer the most likely energies of the precipitating electrons for our model atmospheres. The values are 45–55 keV, 25–30 keV, and 15–20 keV for models A, B, and C, respectively. Our models also show that the column density of H_2 derived by *Wolven and Feldman* [1998] from Werner band emissions terminating on $v = 2$ in auroral spectra recorded by HUT implies an electron energy of about 30 keV.

We have calculated ion production rate profiles and steady state ion density profiles for the auroral regions. Our predicted profiles of hydrocarbon ions are similar to those predicted by *Kim and Fox* [1994] for midlatitudes at local noon, but the densities are an order of magnitude larger. Significant ionization extends down to altitudes near 300 km (3.3 μbar).

We have modeled electron-impact excitation rates of the electronic states of H_2 that emit in the Lyman and Werner bands, that of the H($2p$) state that emits at Lyman alpha, and the Balmer alpha and beta emission rates. We have examined the chemistry of H atoms in detail and present upper limits to the density profiles for H for several combinations of models and electron energy. The predicted peak and integrated densities decrease as the energy of the precipitating electrons increase and as the eddy diffusion coefficient increases. We find, however, that we cannot reproduce the low H column densities of $(1-5) \times 10^{16}$ cm^{-2} that are derived by *Prangé et al.* [1997] from analysis of the self-reversed profile of the auroral Lyman alpha line. Our computed values are, of course, upper limits, which may be re-

duced by winds from the polar to equatorial regions, but such winds cannot reduce the auroral H column densities below their equatorial or midlatitude values, which are in the range $(1-5) \times 10^{17}$ cm^{-2}.

Finally, we find that the temperatures at the altitude of peak electron energy deposition for our Galileo-based thermospheric models are less than 200 K and are much smaller than those derived from rotational analysis of HST data. We conclude that the auroral thermosphere is considerably hotter in the 0.5-10 μbar region than the near-equatorial region that was sampled by the Galileo probe [*Seiff et al.*, 1997] and from which our pressure and temperature profiles were constructed. Calculations for a background model with a more realistic auroral temperature profile are in progress.

Acknowledgments. We thank the referees for their detailed comments, which greatly improved this manuscript. This work has been supported in part by NASA grant NAG56007 to the Research Foundation of the State University of New York at Stony Brook. Partial support was provided by NASA through grant GO-5424 from the Space Telescope Science Institute, which is operated by the Association of Universities for Research in Astronomy, Inc., under NASA contract NAS5-26555. Y.H.K. acknowledges support from the Korea Science and Engineering Foundation (96-0702-03-01-3).

References

Abgrall, H., E. Roueff, F. Launay, J. Y. Roncin, and J. L. Subtil, Table of the Lyman band system of molecular hydrogen, *Astron. Astrophys. Suppl., 101*, 273–321, 1993a.

Abgrall, H., E. Roueff, F. Launay, J. Y. Roncin, and J. L. Subtil, Table of the Werner band system of molecular hydrogen, *Astron. Astrophys. Suppl., 101*, 323–362, 1993b.

Achilleos, N., S. Miller, J. Tennyson, A. D. Aylward, I. Mueller-Wodarg, and D. Rees, JIM: A time-dependent, three-dimensional model of Jupiter's thermosphere and ionosphere, *J. Geophys. Res, 103*, 20,089–20,112, 1998.

Adamczyk, B., A. J. H. Boerboom, B. L. Schram, and J. Kistemaker, Partial ionization cross sections of He, Ne, H_2, and CH_4 for electrons from 20 to 500 eV, *J. Chem. Phys., 44*, 4640, 1966.

Ajello, J. M., et al., Simple ultraviolet calibration source with reference spectra and its use with the Galileo orbiter ultraviolet spectrometer, *Appl. Opt., 27*, 890, 1988.

Ajello, J. M., D. E. Shemansky, and G. K. James, Cross sections for production of H($2p, 2s, 1s$) by electron collisional dissociation of H_2, *Astrophys. J., 371*, 422, 1991.

Ajello, J. M., et al., Galileo orbiter ultraviolet observations of Jupiter aurora, *J. Geophys. Res., 103*, 20,125–20,148, 1998.

Allan, M., Experimental observation of structures in the energy dependence of vibrational excitation in H_2 by electron impact in the $^2\Sigma_u^+$ resonance region, *J. Phys. B At. Mol. Phys., 18*, L451, 1985.

Allen, M., Y. L. Yung, and G. R. Gladstone, The relative abundance of ethane to acetylene in the jovian stratosphere, *Icarus, 100*, 527, 1992.

Anderson, S. M., A. Freedman, and C. E. Kolb, Fast flow studies of CH radical kinetics at 290 K, *J. Phys. Chem., 91*, 6272, 1987.

Anicich, V. G., Evaluated bimolecular ion-molecule gas phase kinetics of positive ions for use in modeling the chemistry of planetary atmospheres, cometary comae, and interstellar clouds, *J. Chem. Phys. Ref. Data, 22*, 1469, 1994.

Atreya, S. K., *Atmospheres and Ionospheres of the Outer Planets and Their Satellites*, 224 pp., Springer-Verlag, New York, 1986.

Atreya, S. K., T. M. Donahue, and J. H. Waite Jr., An interpretation of jovian electron density profiles, *Nature, 280*, 795, 1979.

Atreya, S. K., T. M. Donahue, and M. C. Festou, Jupiter: Structure and composition of the upper atmosphere, *Astrophys. J., 247* L43, 1981.

Ballester, G., et al., Time-resolved observations of Jupiter's far-UV aurora, *Science, 274*, 409–413, 1996.

Bates, D. R, and A. Dalgarno, Electron recombination, in *Atomic and Molecular Processes*, pp.245-271, Academic Press, San Diego, Calif., 1962.

Baulch, D. L., et al., Evaluated kinetic data for combustion modelling, *J. Phys. Chem. Ref. Data, 21*, 411, 1992.

Ben Jaffel, L., J. T. Clarke, R. Prangé, G. R. Gladstone, and A. Vidal-Madjar, The Lyman alpha bulge of Jupiter: Effects of non-thermal velocity field, *Geophys. Res. Lett., 20*, 747-750, 1993.

Berman, M. R., and M. C. Lin, Kinetics and mechanisms of the reactions of CH with CH_4, C_2H_6, and n-C_4H_{10}, *Chem. Phys., 82*, 435, 1983.

Berman, M. R., and M. C. Lin, Kinetics and mechanisms of the reactions of CH and CD with H_2 and D_2, *J. Chem. Phys., 81*, 5743, 1984.

Böhland, T., F. Temps, and H. G. Wagner, The contributions of intersystem crossing and reaction in the removal of $CH_2(\tilde{a}A_1)$ by hydrocarbons studied with the LMR, *Ber. Bunsenges. Phys. Chem., 89*, 1013, 1985.

Böhland, T., F. Temps, and H. G. Wagner, Kinetics of the reactions of $CH_2(\tilde{X}\ ^3B_1)$ radicals with C_2H_2, and C_4H_2 in the temperature range 296 K $\leq T \leq$ 700 K, in *Twenty-First International Symposium on Combustion*, pp. 841–850, Combust. Inst., Pittsburgh, Pa., 1986.

Braun, W., A. M. Bass, and M. Pilling, Flash photolysis of ketene and diazomethane: The production and reaction kinetics of triplet and singlet methylene *J. Chem. Phys., 52*, 5131, 1970.

Broadfoot, A. L., B. R. Sandel, D. E. Shemansky, J. C. McConnell, G. R. Smith, J. B. Holberg, S. K. Atreya, T. M. Donahue, D. F. Strobel, and J. L. Bertaux, Overview of the Voyager ultraviolet spectrometer results through Jupiter encounter, *J. Geophys. Res., 86*, 8259, 1981.

Caldwell, J. J., A. T. Tokunaga, and F. C. Gillett, Possible infrared aurorae on Jupiter, *Icarus, 44*, 667–675, 1980.

Caldwell, J. J., A. T. Tokunga, and G. S. Orton, Further observations of 8 μmpolar brightenings of Jupiter, *Icarus, 53*, 133–140, 1983.

Callaway, J., and K. Unnikrishnan, Electron impact excitation of the $n = 3$ states of hydrogen at intermediate energies, *J. Phys. B At. Mol. Phys., 26*, L419, 1993.

Chatham, H., D. Hils, R. Robertson, and A. Gallagher, Total and partial electron collisional ionization cross sections for CH_4, C_2H_6, SiH_4, and Si_2H_6, *J. Chem. Phys., 81*, 1770, 1984.

Clarke, J. T., H. A. Weaver, P. D. Feldman, H. W. Moos, W. G. Fastie, and C. B. Opal, Spatial imaging of hydrogen Lyman alpha emission from Jupiter, *Astrophys. J., 240*, 696–701, 1980.

Clarke, J. T., J. Trauger, and J. H. Waite Jr., Doppler shifted Ly α emission from Jupiter's aurora, *Geophys. Res. Lett., 16*, 587, 1989.

Clarke, J. T., L. Ben Jaffel, A. Vidal-Madjar, G. R. Gladstone, J. H. Waite Jr., R. Prangé, J.-C. Gérard, J. Ajello, and G. James, Hubble Space Telescope Goddard high-resolution spectrograph H_2 rotational spectra of Jupiter's aurora, *Astrophys. J., 430*, L73, 1994.

Clarke, J. T., et al., Far-ultraviolet imaging of Jupiter's aurora and the Io footprint, *Science, 274*, 404–409, 1996.

Clow, R. P., and J. H. Futrell, Ion-molecule reactions in isotopic hydrogen by ion cyclotron resonance, *Int. J. Mass Spectrom. Ion Phys., 10*, 405, 1972.

Cobos, C. J., and J. Troe, The dissociation recombination system CH_4 + M - reversible - CH_3 + H + M - reevaluated experiments from 300 K to 3000 K, *Z. Phys. Chem. NF, 167*, 129, 1990.

Cook, A. F., A. Vallance Jones, and D. E. Shemansky, Visible aurora in Jupiter's atmosphere?, *J. Geophys. Res., 86*, 8793–8796, 1981.

Cravens, T. E., Vibrationally excited molecular hydrogen in the upper atmosphere of Jupiter, *J. Geophys. Res. 92*, 11,083–11,100, 1987.

Datz, S., G. Sundström, C. Biedermann, L. Broström, H. Danared, S. Mannervik, J. R. Mowat, and M. Larsson, Branching in the dissociative recombination of H_3^+, *Phys. Rev. Lett., 74*, 896–899, 1995.

De Heer, F. J., Electron excitation, dissociation and ionization of H_2, D_2, T_2, simple hydrocarbons and their ions, *Phys. Scr., 23*, 170, 1981.

De Heer, F. J., M. R. C. McDowell, and R. W. Wagenaar, Numerical study of the dispersion relation for e^--H scattering, *J. Phys. B At. Mol. Phys., 10*, 1945, 1977.

Drossart, P., B. Bézard, S. Atreya, J. Lacy, E. Serabyn, A. Tokunaga, and T. Encrenaz, Enhanced acetylene emission in the north pole of Jupiter, *Icarus, 66*, 610-618, 1986.

Drossart, P., J.-P. Maillard, J. Caldwell, S. J. Kim, J. K. G. Watson, W. A. Majewski, J. Tennyson, J. H. Waite Jr., and R. Wagener, Detection of H_3^+ on Jupiter, *Nature, 340*, 539, 1989.

Drossart, P., J.-P. Maillard, J. Caldwell, and J. Rosenqvist, Line-resolved spectroscopy of the Jovian H_3^+ auroral emission at 3.5 μm, *Astrophys. J., 402*, L25-L28, 1993a.

Drossart, P., B. Bezard, S. K. Atreya, J. Bishop, J. H. Waite, and D. Boice, Thermal profiles in the auroral regions of Jupiter, *J. Geophys. Res., 98*, 18,803–18,811, 1993b.

Duncan, C. W., and I. C. Walker, Collision cross sections for low energy electrons in methane, *J. Chem. Soc., 68*, 1514, 1972.

Durrance, S. T., P. D. Feldman, and H. W. Moos, The spectrum of the Jovian aurora 1150–1700 Å, *Geophys. Res. Lett., 9*, 652, 1982.

Ehrhardt, H., L. Langhans, F. Linder, and H. S. Taylor, Resonance scattering of slow electrons from H_2 and CO angular distribution, *Phys. Rev., 173*, 222, 1968.

Emerich, C., L. B. Jaffel, J. T. Clarke, R. Prangé, G. R. Gladstone, J. Sommeria, and G. Ballester, Evidence for supersonic turbulence in the upper atmosphere of Jupiter, *Science, 273*, 1085, 1996.

Eshleman, V. R., G. L. Tyler, G. E. Wood, G. F. Lindal, J. D. Anderson, G. S. Levy, and T. A. Croft, Radio science with Voyager 1 at Jupiter: Preliminary profiles of the atmosphere and ionosphere, *Science, 204*, 976–978, 1979a.

Eshleman, V. R., G. L. Tyler, G. E. Wood, G. F. Lindal, J. D. Anderson, G. S. Levy, and T. A. Croft, Radio science with Voyager 1 at Jupiter: Initial Voyager 2 results and a Voyager 1 measure of the Io torus, *Science, 206*, 959–962, 1979b.

Federer, W., H. Villinger, F. Howorka, W. Lindinger, P. Tosi, D. Bassi, and E. Ferguson, Laboratory studies of ion reactions with atomic hydrogen, in *Molecular Astrophysics*, edited by G. H. F. Diercksen et al., pp. 649-655, D. Reidel, Norwell, Mass., 1985.

Festou, M. C., S. K. Atreya, T. M. Donahue, B. R. Sandel, D. E. Shemansky, and A. L. Broadfoot, Composition and thermal profiles of the Jovian upper atmosphere determined by the Voyager ultraviolet stellar occultation experiment, *J. Geophys. Res., 86*, 5715–5725, 1981.

Frank, P., K. A. Bhaskaran, and T. Just, High temperature reactions of triplet methylene and ketene with radicals, *J. Phys. Chem., 90*, 2226, 1986.

Freund, R. S., J. A. Schiavone, and D. F. Brader, Dissociative excitation of H_2: Spectral line shapes and electron impact cross sections of the Balmer lines, *J. Chem. Phys., 64*, 1122, 1976.

Gérard, J.-C., and V. Singh, A model of energy deposition of energetic electrons and EUV emission in the jovian and saturnian atmospheres and implications, *J. Geophys. Res., 87*, 4525–4532, 1982.

Gérard, J.-C., D. Grodent, R. Prangé, J. H. Waite, G. R. Gladstone, V. Dols, F. Paresce, A. Storrs, L. Ben Jaffel, and K. A. Franke, A remarkable auroral event in Jupiter observed in the ultraviolet with the Hubble Space Telescope, *Science, 266*, 1675-1678, 1994.

Gibson, D. K., The cross section for the J=0–2 rotational excitation of hydrogen by slow electrons, *Aust. J. Phys., 23*, 683, 1970.

Gladstone, G. R., Radiative transfer and photochemistry in the upper atmosphere of Jupiter, Ph.D. Thesis, Calif. Inst. of Technol., Pasadena, 1982a.

Gladstone, G. R., Radiative transfer with partial frequency redistribution in inhomogeneous atmospheres: Application to the Jovian aurora, *J. Quant. Spectrosc. Radiat. Transfer, 27*, 545–556, 1982b.

Gladstone, G. R., and T. E. Skinner, Spectral analysis of Jovian auroral emissions, in *Proceedings of the Workshop on Time-Variable Phenomena in the Jovian System, NASA Spec. Publ., SP-494*, 221, 1989.

Gladstone, G. R., M. Allen, and Y. L. Yung, Hydrocarbon photochemistry in the upper atmosphere of Jupiter, *Icarus, 119*, 1–52, 1996.

Hanel, R., et al., Infrared observations of the Jovian system from Voyager 2, *Science, 206*, 952, 1979.

Hansel, A., R. Richter, W. Lindinger, and E. E. Ferguson, Reactions of C_2 and C_3 hydrocarbon ions with H, D, H_2 and D_2 at near thermal energies, *Int. J. Mass Spectrom. Ion Phys., 94*, 251–260, 1989.

Herbert, F., B. R. Sandel, and A. L. Broadfoot, Observations of the Jovian UV aurora by Voyager, *J. Geophys. Res., 92*, 3141–3154, 1987.

Hinson, D. P., J. D. Twicken, and E. T. Karayel, Jupiter's ionosphere: New results from Voyager 2 radio occultation measurements, *J. Geophys. Res., 103*, 9505–9520, 1998.

Ingersoll, A. P., A. R. Vasavada, B. Little, C. D. Anger, S. C. Bolton, C. Alexander, K. P. Klaasen, W. K. Tobiska, and the Galileo SSI Team, Imaging Jupiter's aurora at visible wavelengths, *Icarus, 135*, 251–264, 1998.

Jackman, C. H., R. H. Garvey, and A. E. S. Green, Electron impact on atmospheric gases, I, Updated cross sections, *J. Geophys. Res., 82*, 5081, 1977.

Jarrold, M. F., L. M. Bass, P. R. Kemper, P. A. M. Van Koppen, and M. T. Bowers, Unimolecular and bimolecular reactions in the $C_4H_6^+$ system: Experiment and theory, *J. Chem. Phys, 78*, 3756, 1983.

Karpas, Z., V. G. Anicich, and W. T. Huntress, An ion cyclotron resonance study of reactions of ions with hydrogen atoms, *J. Chem. Phys., 70*, 2877, 1979.

Kim, J. K., and W. T. Huntress, Ion cyclotron resonance studies on the reaction of H_2^+ and D_2^+ ions with various simple molecules and hydrocarbons, *J. Chem. Phys., 62*, 2820, 1975.

Kim, S. J., Infrared processes in the Jovian auroral zone, *Icarus, 75*, 399–408, 1988.

Kim, S. J., P. Drossart, J. Caldwell, and J.-P. Maillard, Temperatures of the Jovian auroral zone inferred from 2-μm H_2 quadrupole line observations, *Icarus, 84*, 54, 1990.

Kim, Y. H., and J. L. Fox, The chemistry of hydrocarbon ions in the Jovian ionosphere, *Icarus, 112*, 310–325, 1994.

Kim, Y. H., J. L. Fox, and H. A. Porter, H_3^+ in the Jovian ionosphere: densities and vibrational distribution, *J. Geophys. Res., 97*, 6093, 1992.

Kim, Y. H., J. J. Caldwell, and J. L. Fox, High resolution ultraviolet spectroscopy of the Jovian aurora, *Astrophys. J., 447*, 906–914, 1995.

Kim, Y. H., J. L. Fox, and J. J. Caldwell, Temperatures and altitudes of Jupiter's ultraviolet aurora inferred from GHRS observations with the Hubble Space Telescope, *Icarus, 128*, 189–201, 1997.

Kostiuk, T., F. Espenak, and M. J. Mumma, Is ethane varying in the Jovian north polar "Hot spot"?, in *Proceedings of the Workshop on Time-Variable Phenomena in the Jovian System, NASA Spec. Publ., SP-494*, 234–241, 1989.

Kostiuk, T., P. Romani, F. Espenak, T. A. Livengood, and J. J. Goldstein, Temperature and abundances in the Jovian auroral stratosphere, 2, Ethylene as a probe of the microbar region, *J. Geophys. Res., 98*, 18,823–18,830, 1993.

Langford, A. O., H. Petek, and C. B. Moore, Collisional removal of CH_2 ($^1A_1$): Absolute rate constants for atomic and molecular collisional partners at 295 K, *J. Chem. Phys., 78*, 6650, 1983.

Laufer, A. H., and Y. L. Yung, Equivalence of vinylidene and $C_2H_2^*$: Calculated rate constant for vinylidene abstraction from CH_4, *J. Phys. Chem., 87*, 181, 1983.

Lehfaoui, L., C. Rebrion-Rowe, S. Laubé, J. B. A. Mitchell, and B. R. Rowe, The dissociative recombination of hydrocarbon ions, I, Light alkanes, *J. Chem. Phys., 106*, 13, 1997.

Lightfoot, P. D., and M. J. Pilling, Temperature and pressure dependence of the rate constant for the addition of H to C_2H, *J. Phys. Chem., 91*, 3373, 1987.

Lima, M. A. P., T. L. Gibson, W. M. Huo, and V. McKoy, Cross sections for electron impact excitation of the $b^3\Sigma_u^+$ state of H_2: An application of the Schwinger multichannel variational method, *J. Phys. B At. Mol. Phys., 18*, L865, 1985.

Linder, F., and H. Schmidt, Rotational and vibrational excitation of H_2 by slow electron impact, *Z. Naturforsch., 26a*, 1603, 1971.

Liu, W. H., and A. Dalgarno, The ultraviolet spectra of the Jovian aurora, *Astophys. J., 467*, 446, 1996.

Liu, X. M., D. E. Shemansky, S. M. Ahmed, G. K. James, and J. M. Ajello, Electron-impact excitation and emission cross sections of the H_2 Lyman and Werner systems, *J. Geophys. Res., 103*, 26,739–26,758, 1998.

Livengood, T. A., D. F. Strobel, and H. W. Moos, Long-term study of longitudinal dependence in primary particle precipitation in the north Jovian aurora, *J. Geophys. Res., 95*, 10,375–10,388, 1990.

Livengood, T. A., T. Kostiuk, T., F. Espenak, and J. J. Goldstein, Temperature and abundances in the Jovian auroral stratosphere, 2, Ethane as a probe of the millibar region, *J. Geophys. Res., 98*, 18,813–18,822, 1993.

Majeed, T., and J. C. McConnell, The upper ionospheres of Jupiter and Saturn, *Planet. Space Sci., 39*, 1715–1732, 1991.

Majeed, T., J. C. McConnell, and R. V. Yelle, Vibrationally excited H_2 in the outer planets thermosphere: Fluorescence in the Lyman and Werner bands, *Planet. Space Sci., 39*, 1591–1606, 1991.

Mason, N. J., and W. R. Newell, Electron resonance structure observed in the $c^3\Pi_u$ and $B^1\Sigma_u^+$ cross sections of H_2, *J. Phys. B At. Mol. Phys., 19*, L203, 1986.

McConnell, J. C., B. R. Sandel, and A. L. Broadfoot, Airglow from Jupiter's nightside and crescent: Ultraviolet spectrometer observations from Voyager 2, *Icarus, 43*, 128–142, 1980.

McElroy, M. B., The ionospheres of the major planets, *Space Sci. Rev., 14*, 460, 1973.

McMahon, T. B., P. G. Miasek, and J. L. Beauchamp, *Int. J. Mass Spectrom. Ion Phys., 21*, 63, 1976.

Metzger, A. E., D. A. Gilman, J. L. Luthey, K. C. Hurley, H. W. Schnopper, F. D. Sweard, and J. D. Sullivan, The detection of x-rays from Jupiter, *J. Geophys. Res., 88*, 7731–7741, 1983.

Miller, S., R. D. Joseph, and J. Tennyson, Infrared emission of H_3^+ in the atmosphere of Jupiter in the 2.1 and 4.0 micron region, *Astrophys. J. Lett., 360*, L55, 1990.

Mitchell, J. B. A., The dissociative recombination of molecular ions, *Phys. Rep., 186*, 216, 1990.

Möhlmann, G. R., and F. J. De Heer, Emission cross sections of the $H_2(3p\ ^3\Pi_u \rightarrow 2s\ ^3\Sigma_g^+)$ transition for electron impact on H_2, *Chem. Phys. Lett., 43*, 240, 1976.

Möhlmann, G. R., and F. J. De Heer, Emission cross sections of the Hα and $CH(A^2\Delta \rightarrow X^2\Pi)$ radiation for electron impact on hydrocarbons, *Chem. Phys. 19*, 233, 1977.

Möhlmann, G. R., K. H. Shima, and F. J. De Heer, Production of H, D(2s,2p) by electron impact (0-2000 eV) on simple hydrogen containing molecules, *Chem. Phys., 28*, 331, 1978.

Morrissey, P. F., P. D. Feldman, J. T. Clarke, B. C. Wolven, D. F. Strobel, S. T. Durrance, and J. T. Trauger, Simultaneous spectroscopy and imaging of the Jovian aurora with the Hopkins Ultraviolet Telescope, and the Hubble Space Telescope, *Astrophys. J., 476*, 918–923, 1997.

Mul, P. M., and J. W. McGowan, Dissociative recombination of C_2^+, C_2H^+, $C_2H_2^+$, and $C_2H_3^+$, *Astrophys. J., 237*, 749, 1980.

Mul, P. M., J. B. A. Mitchell, V. S. D'Angelo, P. Defrance, J. W. McGowan, and H. R. Froelich, Merged electron-ion beam experiments, IV, Dissociative recombination for the methane group CH^+, CH_2^+, CH_3^+, CH_4^+, CH_5^+, *J. Phys. B At. Mol. Phys., 14*, 1353, 1981.

Mumma, M. J., and E. C. Zipf, Dissociative excitation of vacuum ultraviolet emission features by electron impact on molecular gases, I, H_2 and O_2, *J. Chem. Phys., 55*, 1661, 1971.

Munk, J., P. Pagsberg, E. Ratajczak, and A. Sillesen, Spectrokinetic studies of ethyl and ethylperoxy radicals, *J. Phys. Chem., 90*, 2752, 1986.

Niemann, H. B., et al., The Galileo probe mass spectrometer: Composition of Jupiter's atmosphere, *Science, 272*, 846–849, 1996.

Oka, T., and T. R. Geballe, Observations of the 4 micron fundamental band of H_3^+ in Jupiter, *Astrophys. J., 351*, L53–L56, 1990.

Pang, K. D., J. M. Ajello, and B. Franklin, Electron impact excitation cross section studies of methane and acetylene, *J. Chem. Phys., 86*, 2750, 1987.

Phillips Petroleum Co., Thermodynamics Research Center Hydrocarbon Project, *Selected Mass Spectral Data*, College Station, Texas, 1983.

Porter, H. S., F. Varosi, and H. G. Mayr, Iterative solution of the multistream electron transport equation, 1, Comparison with laboratory beam injection experiments, *J. Geophys. Res., 92*, 5933–5959, 1987.

Prangé, R., D. Rego, L. Pallier, L. Ben Jaffel, C. Emerich, J. Ajello, J. T. Clarke, and G. E. Ballester, Detection of self-reversed Lyα line from the Jovian aurorae, with the Hubble Space Telescope, *Astrophys. J., 484*, L169–L173, 1997.

Pryor, W. R., and C. W. Hord, A study of photopolarimeter system UV absorption data on Jupiter, Saturn, Uranus, and Neptune: Implications for auroral haze formation, *Icarus, 91*, 161–172, 1991.

Rapp, D., and P. Englander-Golden, Total cross sections for ionization and attachment in gases by electron impact, I, Positive ionization. *J. Chem. Phys., 43*, 1464, 1965.

Rebrion-Rowe, C., L. Lehfaoui, B. R. Rowe, and J. B. A. Mitchell, The dissociative recombination of hydrocarbon ions, II, Alkene and alkyne derived species, *J. Chem. Phys., 108*, 7185, 1998.

Rego, D., R. Prangé, and J.-C. Gérard, Auroral Lyman alpha and H_2 bands from the giant planets, 1, Excitation by proton precipitation in the Jovian atmosphere, *J. Geophys. Res., 99*, 17,075–17,094, 1994.

Sandel, B. R., et al., Extreme ultraviolet observations from Voyager 2 encounter with Jupiter, *Science, 206*, 962, 1979.

Schauer, M. M., S. R. Jefferts, S. E. Barlow, and G. H. Dunn, Reactions of H_2 with He^+ at temperature below 40 K, *J. Chem. Phys., 91*, 4593, 1989.

Scott, M. P., T. T. Scholz, H. R. J. Walters, and P. G. Burke, Electron scattering by atomic hydrogen at intermediate energies, I, Integrated elastic, 1s–2s and 1s–2p cross sections, *J. Phys. B At. Mol. Phys., 22*, 3055, 1989.

Seiff, A, D. B. Kirk, T. C. D. Knight, L. A Young, F. S Milos, E. Venkatapathy, J. D. Mihalov, R. C. Blanchard, R. E. Young, and G. Schubert, Thermal structure of Jupiter's upper atmosphere, derived from the Galileo Probe, *Science, 276*, 102–104, 1997.

Semaniak, J., et al., Dissociative recombination and excitation of CH_5^+: Absolute cross sections and branching fractions, *Astrophys. J., 498*, 886, 1998.

Shemansky, D. E., J. M. Ajello, and D. T. Hall, Electron impact excitation of H_2: Rydberg band system and the benchmark dissociative cross section for H Lyman-alpha, *Astrophys. J., 296*, 765, 1985.

Singhal, R. P., S. C. Chakravarty, A. Bhardwaj, and B. Prasad, Energetic electron precipitation in Jupiter's upper atmosphere, *J. Geophys. Res., 97*, 18,245–18,256, 1992.

Skinner, T. E., S. T Durrance, P. D. Feldman, and H. W. Moos, Temporal variation of the Jovian H I Lyman alpha emission (1979–1982), *Astrophys. J., 265*, L23–L27, 1983.

Skinner, T. E., S. T. Durrance, P. D. Feldman, and H. W. Moos, IUE observations of longitudinal and temporal variations in the Jovian auroral emission, *Astrophys. J., 278*, 441, 1984.

Skinner, T. E., M. T. DeLand, G. E. Ballester, K. A. Coplin, P. D. Feldman, and H. W. Moos, Temporal variation of the Jovian H I Lyman alpha emission, *J. Geophys. Res., 93*, 29–34, 1988.

Space Telescope Science Institute, The Goddard High Resolution Spectrograph, in *HST Data Handbook*, Space Telescope Science Institute, Baltimore, 1994.

Stephens, J. W., J. L. Hall, H. Solka, W.-B. Yan, R. F. Curl, and G. P. Glass, Rates constant measurements of reactions of C_2H with H_2, O_2, C_2H_2, and NO using color center laser kinetic spectroscopy, *J. Phys. Chem., 91*, 5740, 1987.

Sundström, G., et al., Destruction rate of H_3^+ by low energy electrons measured in a storage-ring experiment, *Science, 263*, 785–787, 1994.

Tanaka, H., Experimental results in electron-molecule inelastic collision experiments, *Lect. Notes Chem., 35*, 6, 1984.

Teng, L., and W. E. Jones, Kinetics of the reactions of hydrogen atoms with ethylene and vinyl fluoride, *J. Chem. Soc. Faraday Trans., 1, 68*, 1267, 1972.

Trafton, L. M., J.-C. Gérard, G. Munhoven, and J. H. Waite, High resolution spectra of Jupiter's northern auroral ultraviolet emission with the Hubble Space Telescope, *Astrophys. J., 421*, 816–827, 1994.

Trafton, L. M., V. Dols, J.-C. Gerard, J. H. Waite, G. R. Gladstone, and G. Mundhoven, HST spectra of the Jovian ultraviolet aurora: Search for heavy ion precipitation, *Astrophys. J., 507*, 955–967, 1998.

Tsang, W., Rate constants for the decomposition and formation of simple alkanes over extended temperature and pressure ranges, *Combust. Flame, 78*, 71, 1989.

Tsang, W., and R. F. Hampson, Chemical kinetic data-base for combustion chemistry, 1, Methane and related compounds, *J. Phys. Chem. Ref. Data, 15*, 1087, 1986.

Von Zahn, U., and D. M. Hunten, The helium mass fraction in Jupiter's atmosphere, *Science, 272*, 849–851, 1996.

Vuskovic, L., and S. Trajmar, Electron impact excitation of methane, *J. Chem. Phys., 78*, 4947, 1983.

Waite, J. H., Jr., T. E. Cravens, J. U. Kozyra, A. F. Nagy, S. K. Atreya, and R. H. Chen, Electron precipitation and related aeronomy of the Jovian thermosphere and ionosphere, *J. Geophys. Res., 88*, 6143, 1983.

Waite, J. H., Jr., J. T. Clarke, T. E. Cravens, and C. M. Hammond, The Jovian aurora: Electron or ion precipitation? *J. Geophys. Res., 93*, 7244–7250, 1988.

Waite, J. H., Jr., F. Bagenal, F. Seward, C. Na, G. R. Gladstone, T. E. Cravens, K. C. Hurley, J. T. Clarke, R. Elsner, and S. A. Stern, ROSAT observations of the Jupiter aurora, *J. Geophys. Res., 99*, 14,799, 1994.

Winters, H. F., Dissociation of methane by electron impact, *J. Chem. Phys., 63*, 3462, 1975.

Wolven, B. C., and P. D. Feldman, Self-absorption by vibrationally excited H_2 in the Astro-2 Hopkins Ultraviolet Telescope spectrum of the jovian aurora, *Geophys. Res. Lett., 25*, 1537–1540, 1998.

Yung, Y. L., G. R. Gladstone, K. M. Chang, J. M. Ajello, and S. K. Srivastava, H_2 fluorescence spectrum from 1200 to 1700 Å by electron impact: Laboratory study and application to Jovian aurora, *Astrophys. J. Lett., 254*, L65, 1982.

Zeng, S. H., and S. K. Srivastava, Electron-impact ionization and dissociative ionization of acetylene, *J. Phys. B At. Mol. Opt. Phys., 29*, 3235, 1996.

J. L. Fox, Department of Physics, Wright State University, Dayton, OH 45435. (fox@platmo.phy.wright.edu)

Y. H. Kim, Department of Astronomy and Space Science, Chungnam National University, Daejon, Korea. (ykim@jupiter.chungnam.ac.kr)

J. J. Perry, AODTRA/CPTIP, 1680 Texas Street, SE, Kirtland AFB, NM 87117.

H. S. Porter, Department of Computer Science, Furman University, Greenville, SC 29613.

(Received November 4, 1998; revised March 3, 1999; accepted March 8, 1999.)